December 2008

Guided Assembly of Nanostructures via Elastic Interactions

John L. Bassani
University of Pennsylvania, bassani@seas.upenn.edu

Youcun Lou
University of Pennsylvania

Postprint version. Published in *Journal of the Mechanics and Physics of Solids*, Volume 56, Issue 12, December 2008, pages 3507-3526.
Publisher URL: http://dx.doi.org/10.1016/j.jmps.2008.08.009

Guided Assembly of Nanostructures via Elastic Interactions

Abstract
A solid solution can spontaneously separate into phases that self-assemble into patterns. This process can be guided via external fields to form ordered micro- and nanostructures. In this paper, we demonstrate that notions of interaction energies provide powerful insights into the coupling of these fields with the properties of the alloy. A phase-field model is developed that incorporates chemical, interfacial, and elastic energies, including heterogeneous elastic properties, and couples naturally to externally imposed mechanical fields. Aggregation in bulk and in thin films under patterned external load is investigated. The kinetics and morphology of phase separation are shown to depend significantly on elastic properties of the system, which include elastic heterogeneity and the misfit or transformation strain. Eshelby-type asymptotic estimates for interaction energies are shown to be very useful in understanding and predicting the trends observed from the simulations.

Keywords
guided assembly, phase-field model, elastic interactions

Comments
Postprint version. Published in *Journal of the Mechanics and Physics of Solids*, Volume 56, Issue 12, December 2008, pages 3507-3526.
Publisher URL: http://dx.doi.org/10.1016/j.jmps.2008.08.009

Guided Assembly of Nanostructures via Elastic Interactions

Yucun Lou and John L. Bassani

Department of Mechanical Engineering and Applied Mechanics

University of Pennsylvania, Philadelphia, PA, 19014

June 2008

Abstract

A solid solution can spontaneously separate into phases that self assemble into patterns. This process can be guided via external fields to form ordered micro- and nano-structures. In this paper, we demonstrate that notions of interaction energies provide powerful insights into the coupling of these fields with the properties of the alloy. A phase field model is developed that incorporates chemical, interfacial, and elastic energies, including heterogeneous elastic properties, and couples naturally to externally-imposed mechanical fields. Aggregation in bulk and in thin films under patterned external load are investigated. The kinetics and morphology of phase separation are shown to depend significantly upon elastic properties of the system, which include elastic heterogeneity and the misfit or transformation strain. Eshelby-type asymptotic estimates for interaction energies are shown to be very useful in understanding and predicting the trends observed from the simulations.

1. Introduction

An initially homogeneous solid solution (e.g., a binary alloy) at high temperature can be quenched and aged to cause phase separation (precipitation or spinodal decomposition).

Precipitates can self assemble into patterns, e.g., ordered clusters, on the scale of micro- to nano-meters. This phenomenon has been widely observed, e.g., in Ag-Ru alloys (Pohl et al., 1999) and in Cu-Pb alloys (Plass and Kellogg, 2000) to cite two systems out of many. The ability to guide the aggregation process offers tremendous possibilities for designing and fabricating devices, including quantum dots, nano sensor arrays, data storage, and molecular electronics. One approach is to grow nanostructures epitaxially on soft or hard templates, for example, DNA coated nanostructures (Patolsky et al., 2002) or mesoporous silica (Wu et al., 2004). However, the utilization of these methods has been limited because the mechanisms are unclear and often the cost of templates is prohibitive.

External fields, e.g., elastic, electric, and magnetic fields, have been shown to also bias the assembly process. For example, Hung et al. (1999) applied a uniform external stress to affect the morphology of precipitates in metal alloy films. Velev et al. (2003) directed motion of nanoparticles using an external electric field. Ahniyaz et al. (2007) fabricated highly oriented superlattices by inducing an external magnetic field. These experimental findings suggest the possibility of directing precipitation to form patterned microstructures through the application of non-uniform external fields.

Technological advances that utilize patterned external fields to control the formation of nanostructures inevitably will require a fundamental understanding of underlying mechanisms as well as basic engineering design principles based upon mathematical models. Possible modeling approaches include molecular dynamics and Monte Carlo simulations, but both generally are limited by accessible spatial and temporal scales. Continuum methods with

physically-based constitutive models offer possibilities to increase the simulation domain and time. Among such methods the so-called sharp interface model treats the heterogeneous system as two or more different phases separated by mathematically sharp interfaces (e.g., see Kawasaki and Enomoto, 1988; Doi, 1996; Thornton et al, 2003), but this requires specification of a kinetic relation for the propagating interfaces. Phase field models do not, and they also overcome the challenge of interface tracking by employing continuous field variables that can describe bulk as well as interfacial phases.

Cahn and Hilliard (1958) introduced a phase field model to investigate properties of interfaces, especially the dependence of interfacial thickness on temperature. In their pioneering work, the free energy density was taken to depend not only upon field variables, e.g., concentrations, but also gradients of those variables in order to account for the interfacial energy. Many applications of phase field models followed Cahn and Hilliard (see Chen, 2002; Thornton et al, 2003), and no attempt at comprehensive review is made here. More recently, Eggleston and Voorhees (2001) studied the equilibrium morphologies of precipitates affected by the anisotropy of interfacial energy. The influence of elastic energy can be readily incorporated in a phase field model, but nearly all studies in the literature that include elastic effects assume that the material properties are uniform, i.e., the same in the matrix and precipitate. For example, Chen and coworkers (Li and Chen, 1998; Vaithyanathan and Chen, 2002) investigated the effect of uniform external load on the alignment of precipitates including the effects of transformation (or misfit) strain in an elastically homogeneous system. Wen et al (2006) studied the effect of temperature on the kinetics of coarsening in an elastically homogeneous 3D bulk. Suo and Lu (2000)

investigated aggregation in a binary epilayer that induces elastic straining in a coherent (and elastically homogeneous) substrate. Johnson and Wise (2002) and Wise et al. (2005) studied the effects of surface energy on aggregation in stressed thin films including the effects of patterned substrates but also with elastic homogeneity.

The influence of elastic heterogeneity on the evolution of microstructure has been the subject of only a few studies. For example, Chen and coworkers (Hu and Chen, 2001; Zhu et al., 2001) observed that the kinetics of coarsening and the elongation of precipitates in an alloy with a very high concentration of solute (50%) is affected by elastic heterogeneity. In a recent investigation, Gururajan and Abinandanan (2007) found that the coarsening and coalescence of precipitates are accelerated when precipitate phase is softer than matrix phase and when the uniform external load has the same sign as the transformation strain. However, a systematic investigation of the effects of both transformation strain and elastic contrast as well as a theoretical understanding of these effects is lacking.

In this paper we adopt a Cahn-Hilliard model that naturally allows coupling with externally-imposed mechanical fields to study aggregation in the bulk and in thin films under patterned loads. Our work differs from most of aforementioned studies in several respects. In this paper, the effects of both transformation strains and heterogeneous elastic properties that result from time- and spatially-varying concentration fields during aggregation are investigated systematically for isotropic material behavior. The resulting non-uniform elastic energy density is determined from complete solutions to the Navier equations with continuously varying elastic heterogeneity. No approximations, other than those involved in the numerical algorithm, are

made for the stress and strain fields (Suo and Lu, 2000, for example, assumed a linear dependence of the film stress on local concentration). As a result, the stiffness matrix must be assembled and inverted at each time step, which is the most time-consuming part of the computation. From extensive simulations, the magnitude of the transformation strain and the overall contrast in elastic heterogeneity are shown to significantly affect the kinetics of aggregation in the bulk, even in the absence of load, and the kinetics and morphology in thin films under patterned loads; in the latter case there also is a strong dependence on the sign of the transformation strain as well. All these observations are interpreted in detail in terms of Eshelby-type estimates for elastic self and interaction energies between precipitates and with externally applied stress. Even though these estimates apply rigorously only in the dilute and small contrast limits, remarkably they can be interpreted to explain the observed trends and, therefore, have potential to provide design guidelines to control the formation of nanostructures by diffusional phase separation in a wide range of material systems.

In the next section, a phase field model is developed that couples externally-imposed stress field. In Sec. 3, the constitutive models for chemical energy, interfacial energy, transformation strain, and effective elastic modulus are discussed in detail. The numerical implementation is discussed in Sec. 4, and simulations of aggregation in the 2D bulk and in thin films are investigated in Sec. 5 and 7, respectively. Those results are interpreted following Eshelby's ideas for the self and interaction energies, which are developed in Sec. 6.

2. Phase field model

Consider a binary mixture that phase separates with the following characteristics:

i) the formation of precipitates (minority phases) can induce a transformation strain;

ii) the elastic properties of the system can be heterogeneous;

iii) an excess energy is associated with interfacial regions.

A continuous field variable c is introduced to represent the concentration (volume fraction) of minority species in a binary mixture. The free-energy density, f, of the material is assumed to depend upon c, ∇c and the strain field $\boldsymbol{\varepsilon}$ [1]. Following the work Cahn and Hilliard (1958), the leading term of $f\left(c,\nabla c,\boldsymbol{\varepsilon}\right)$ in an isotropic material is expressed as

$$f\left(c,\nabla c,\boldsymbol{\varepsilon}\right)=W\left(c\right)+\gamma\,\nabla c\cdot\nabla c+E\left(\boldsymbol{\varepsilon},c\right)\quad . \tag{2.1}$$

For an isothermal process, the chemical energy density, $W\left(c\right)$, is the Gibbs free energy of a homogenous material with concentration c, which typically is governed by a multi-well potential. The second term on the right-hand side of (2.1) approximates the excess interfacial energy; in general $\gamma\left(c\right)$, but in this work γ is taken to be constant. The third term $E\left(\boldsymbol{\varepsilon},c\right)$ represents elastic energy density. The total strain, $\boldsymbol{\varepsilon}$, is the sum of the elastic strain associated with stress plus a transformation strain which, along with the elastic properties, in general depends upon c.

Aggregation is a non-equilibrium thermodynamic process during which the free energy tends to monotonically decrease as material redistributes. The mass flux, **J**, is assumed to be proportional to the gradient of chemical potential, μ, that is defined by variations in local free

[1] Boldface symbols denote tensor variables.

energy density with respect to compositional variations (Mullins, 1957). Therefore,

$$\mathbf{J} = -M\nabla\mu = -M\nabla\left(\frac{\partial f}{\partial c}\right) \quad , \tag{2.2}$$

where M is the mobility[2]. Mass conservation leads to

$$\frac{\partial c}{\partial t} = -\nabla\cdot\mathbf{J} \quad . \tag{2.3}$$

With (2.1) and (2.2) the governing nonlinear diffusion equation (2.3) is:

$$\frac{\partial c}{\partial t} = M\nabla^2\left[\frac{dW(c)}{dc} - 2\gamma\nabla^2 c + \frac{\partial E(\varepsilon_{ij}, c)}{\partial c}\right] \quad . \tag{2.4}$$

The elastic energy density, E, is associated with an equilibrium stress field that is related to the elastic strain through a constitutive equation. The total strain is the sum of the elastic strain, which is taken to be linearly related to stress, plus a transformation strain:

$$\varepsilon_{ij} = \varepsilon_{ij}^{\mathrm{e}} + \varepsilon_{ij}^{\mathrm{T}} = \tilde{M}_{ijkl}\sigma_{kl} + \varepsilon_{ij}^{\mathrm{T}} \quad , \tag{2.5}$$

where $\varepsilon_{ij}^{\mathrm{e}}$ and $\varepsilon_{ij}^{\mathrm{T}}$ represent the elastic and transformation strains, respectively, and $\tilde{M}_{ijkl}$ and its inverse $\tilde{C}_{ijkl}$ are tensors of *effective* elastic compliance and stiffness (modulus), respectively, that depend on local concentration of solute. In general, the transformation strain and the effective modulus tensors are functions of c, and explicit approximations are given in the next section. The elastic strain energy density is:

$$E(\varepsilon_{ij}, c) = \frac{1}{2}\left(\varepsilon_{ij} - \varepsilon_{ij}^{\mathrm{T}}\right)\tilde{C}_{ijkl}\left(\varepsilon_{kl} - \varepsilon_{kl}^{\mathrm{T}}\right) \quad . \tag{2.6}$$

For small deformations the total (compatible) strain is derived from displacement field as

---

[2] In general, the mobility is a second-order tensor, but in this work we consider only isotropic behavior in which case the mobility is a scalar quantity.

$$\varepsilon_{ij} = \frac{1}{2}\left(u_{i,j} + u_{j,i}\right) \quad . \tag{2.7}$$

In the absence of body and inertial forces, overall equilibrium, $\sigma_{ij,j} = 0$, is expressed in terms of the displacement field using (2.5) and (2.7) that leads to the Navier equations:

$$\left\{\tilde{C}_{ijkl}\left[\frac{1}{2}\left(u_{k,l} + u_{l,k}\right) - \varepsilon^{\mathrm{T}}_{kl}\right]\right\}_{,j} = 0 \quad . \tag{2.8}$$

An important aspect of the class of problems considered in this paper is the fact that spatial variations of the elastic properties, $\tilde{\mathbf{C}}(\mathbf{x})$, and transformation strain, $\boldsymbol{\varepsilon}^{\mathrm{T}}(\mathbf{x})$, contribute to gradients in the Navier equations (2.8).

3. Constitutive equations

Constitutive relations for the chemical energy, interfacial energy, transformation strain, and effective elastic modulus are key ingredients of the phase field model outlined in Sec. 2. These relations are discussed in the following subsections.

3.1 Chemical energy

Phase separation in a binary alloy naturally occurs in a system described by a free-energy function of the form (2.1) with a chemical energy defined by a double-well potential as a function of concentration. For example, from regular solution theory (Guggenheim, 1952):

$$\begin{aligned} W(c) = \frac{s}{2}\Big[& \varepsilon_{\mathrm{mm}} c^2 + \varepsilon_{\mathrm{pp}}(1-c)^2 + \varepsilon_{\mathrm{pm}} c(1-c)\Big] \\ & + k_B T\Big[c\ln c + (1-c)\ln(1-c)\Big] \end{aligned} \quad , \tag{3.1}$$

where $\varepsilon_{\mathrm{pp}}$, $\varepsilon_{\mathrm{mm}}$, and $\varepsilon_{\mathrm{pm}}$ represent the chemical bonding energies, respectively, between precipitate-precipitate, matrix-matrix and precipitate-matrix; s represents the number of nearest neighbors per atom/molecule; k_B is Boltzmann's constant; and T represents temperature, which is

taken to be uniform in this study. Equilibrium solute concentrations of precipitate and matrix phase, represented by c_{p} and c_{m}, respectively, are obtained from solutions to the quadratic equation:

$$\frac{d\,W(c)}{d\,c} = k_B T \ln\left(\frac{c}{1-c}\right) + s\varepsilon(1-2c) = 0 \quad , \tag{3.2}$$

where,

$$\varepsilon = \varepsilon_{\mathrm{pm}} - \frac{1}{2}\left(\varepsilon_{\mathrm{pp}} + \varepsilon_{\mathrm{mm}}\right) \quad . \tag{3.3}$$

Since the diffusion process governed by (2.4) depends only upon higher-order gradients of $W(c)$, the linear terms in (3.1) that account for distinct well depths can be omitted and it is sufficient to consider:

$$W(c) = k_B T\left[c\ln c + (1-c)\ln(1-c)\right] + s\varepsilon c(1-c) \quad . \tag{3.4}$$

A simpler expression for a double-well potential W (c) was proposed by Ginzburg and Landau (1950):

$$W(c) = w_{\mathrm{o}}\left(c-c_{\mathrm{p}}\right)^2\left(c-c_{\mathrm{m}}\right)^2 \quad , \tag{3.5}$$

where w_{o}, c_{p} and c_{m} are constant. The phenomenological expression (3.5) reasonably approximates regular solution theory (3.4) as shown Fig. 1 for the case $c_{\mathrm{p}} = 1 - c_{\mathrm{m}}$ with the same energy at $c = c_{\mathrm{p}}$, $c = c_{\mathrm{m}}$, and $c = 1/2$. Furthermore, the Ginzburg-Landau form can readily be extended to systems involving more than two phases:

$$W(c) = w_{\mathrm{o}}\left(c-c_1\right)^2\left(c-c_2\right)^2\left(c-c_3\right)^2 \ldots \quad , \tag{3.6}$$

as well as different energy levels for each phase:

$$W(c) = w_{\mathrm{o}}\left(c-c_{\mathrm{m}}\right)^2\left[\left(c-c_{\mathrm{p}}\right)^2 + A\right] \quad , \tag{3.7}$$

where A is a constant.

In the present study we adopt the phenomenological Ginzburg-Landau potential. For convenience, we replace *c* with a scaled volume fraction that is zero in the ideal matrix phase and 1 in the ideal precipitate phase:

$$\phi = \frac{c - c_{\mathrm{m}}}{c_{\mathrm{p}} - c_{\mathrm{m}}} \quad . \tag{3.8}$$

In terms of ϕ, (3.5) becomes

$$W(\phi) = w_{\mathrm{o}} \left(c_{\mathrm{p}} - c_{\mathrm{m}}\right)^4 \phi^2 (1-\phi)^2 \quad . \tag{3.9}$$

3.2 Interfacial energy

The coefficient γ in (2.1) can be related to the interfacial energy density, Γ_{int}. Neglecting dependence of elastic energy on concentration, Cahn and Hilliard (1958) have shown for 1D or for radially-symmetric 2D or 3D precipitates that (see also Wheeler et al., 1992 and Elder et al., 2001):

$$\Gamma_{\mathrm{int}} = 2\sqrt{\gamma} \int_0^1 \sqrt{W(\phi)}\, \mathrm{d}\phi \tag{3.10}$$

For example, with $W(\phi)$ defined in (3.9), γ is determined by the magnitude of the well depth, w_{o}, and the solute concentration in the matrix and precipitate:

$$\gamma^{1/2} = \frac{3\Gamma_{\mathrm{int}} / \sqrt{w_{\mathrm{o}}}}{\left(c_{\mathrm{p}} - c_{\mathrm{m}}\right)^2} \quad . \tag{3.11}$$

As noted by Fried and Gurtin (1994, 1999), (3.10) holds in the sharp interface limit with continuous displacements even when elastic properties depend upon *c*. From the phase-field simulations presented below, estimates of the total interfacial energy (e.g., Fig. 3) are computed from the spatial integral of $\gamma \nabla c \cdot \nabla c$, i.e. the second term on the right-hand side of (2.1).

3.3 Transformation strain

A transformation strain (also referred to as a misfit or eigen strain) associated with phase separation generally arises from differences in the molecular structure of the precipitate and matrix. This strain can, in general, involve both dilation and shear. Since only isotropic elastic and interface properties are considered in this study, the transformation strain is taken to be purely dilatational, i.e.:

$$\varepsilon_{ij}^{\mathrm{T}}(c) = g^{\mathrm{T}}(c)\delta_{ij} \quad , \tag{3.12}$$

where δ_{ij} is Kronecker delta function.

The transformation strain is defined to be zero in the matrix phase, and since the double-well chemical energy leads to phase separation with relatively sharp interfaces, intermediate values of $g^{\mathrm{T}}(c)$ typically are confined to interface regions. For simplicity, $g^{\mathrm{T}}(c)$ is assumed to vary monotonically with maximum magnitude in the precipitate according to:

$$g^{\mathrm{T}}(c) = \begin{cases} \varepsilon^{\mathrm{T}} , & 1 \geq c > c_{\mathrm{p}} \\ \tilde{g}(c)\varepsilon^{\mathrm{T}} , & c_{\mathrm{p}} \geq c \geq c_{\mathrm{m}} \\ 0 , & c_{\mathrm{m}} > c \geq 0 \end{cases} \quad , \tag{3.13}$$

where the transition function $\tilde{g}(c)$ continuously varies from 0 to1 and, therefore, ε^{T} is the maximum value of the transformation strain. A monotonic function with continuous first derivatives at $c = c_{\mathrm{p}}, c_{\mathrm{m}}$ is (Leo et al., 1998):

$$\tilde{g}(c) = 3\left(\frac{c - c_{\mathrm{m}}}{c_{\mathrm{p}} - c_{\mathrm{m}}}\right)^2 - 2\left(\frac{c - c_{\mathrm{m}}}{c_{\mathrm{p}} - c_{\mathrm{m}}}\right)^3 \quad \text{or} \quad \tilde{g}(\phi) = 3\phi^2 - 2\phi^3 \quad . \tag{3.14}$$

Since first derivatives of $\boldsymbol{\varepsilon}^{\mathrm{T}}$ enter the Navier equations, (3.13) with (3.14) are convenient for the simulations that follow.

3.4 Effective elastic moduli

The elastic properties of a multi-phase system are, in general, heterogeneous and spatially vary as a function of concentration. In this work, we imagine that these properties are well defined (i.e., known) for the matrix and precipitate, but the concentration dependent properties in the regions where $c \neq c_{\mathrm{m}}$ or c_{p} (e.g., in the interface regions) are not well known. Here we contemplate continuously varying, local effective elastic moduli, which is different from the classical scenario of composite materials. Therefore, approximations for the effective elastic moduli as a function of concentration, $\tilde{C}_{ijkl}(c)$, are required to evaluate the strain energy density (2.6) at each material point. Estimates commonly adopted for composite materials include mean-field approximations, for example, self-consistent (Budiansky, 1965, Willis, 1977), composite sphere assemblies (Hashin and Shtrikman, 1963), or Mori-Tanaka (1973) estimates. Another approach is to bound the effective properties, for example, Voigtor Reuss bounds (Paul, 1960), or Hashin and Shtrikman (1963) bounds. All these estimates, strictly speaking, are valid only on length scales that are much greater than the scale of the representative microstructure.

For continuously varying solute concentration in the presence of non-uniform mechanical fields, this separation of length scales is not well defined. In general, the length scale of the representative volume element (RVE) is even smaller than the thickness of interfaces surrounding precipitates, which varies from nanometers to micrometers. Therefore, the assumption that the length scale of the RVE is large compared to the scale of the microstructure is no longer valid. Nevertheless, estimates are required for a phase field model that reasonably accounts for effects of elastic energy. Alber et al. (1992, 1996) demonstrated that reasonable

estimates, even on the nanometer scale, for the effective elastic properties of grain boundaries can be computed from atomic-level (molecular static) simulations. They showed that the computed effective moduli are generally within simple bounds for a representative continuum (Alber et al. 1992) and can be used to capture the interfacial waves associated with long-wave-length phonons. That work demonstrated that, at least in the context of grain boundaries, that physically meaningful effective elastic properties can be defined at the nanometer scale. In the remainder of this subsection we motivate simple estimates for $\tilde{C}_{ijkl}(c)$.

In this study, we assume linearly isotropic properties, in which case $\tilde{C}_{ijkl}$ can be expressed in terms of the effective bulk and shear moduli, $\tilde{K}$ and $\tilde{G}$, respectively:

$$\tilde{C}_{ijkl} = \frac{3\tilde{K} - 2\tilde{G}}{3}\delta_{ij}\delta_{kl} + \tilde{G}\left(\delta_{il}\delta_{jk} + \delta_{ik}\delta_{jl}\right) \quad , \tag{3.15}$$

To develop approximations for $\tilde{K}$ and $\tilde{G}$ as a function of c, we begin by considering two limiting states: the nearly uniform state (short time) and well aggregated state (coarsened). The initial state is imagined to be a homogenous solution with solute concentration c_{ave}, and for short times after that every continuum material point is imaged to be a nearly homogeneous mixture with concentration:

$$c(\mathbf{x},t) = c_{\text{ave}} + \delta c(\mathbf{x},t) \quad , \tag{3.16}$$

where δc represents small fluctuations. In this limit, for smooth variations it is reasonable to assume that

$$\begin{aligned} \tilde{K} &= \tilde{K}_{\text{ave}} + K'\,\delta c = \tilde{K}_{\text{ave}} + K'\left(c_{\text{p}} - c_{\text{m}}\right)\delta\phi \\ \tilde{G} &= \tilde{G}_{\text{ave}} + G'\,\delta c = \tilde{G}_{\text{ave}} + G'\left(c_{\text{p}} - c_{\text{m}}\right)\delta\phi \end{aligned} \quad , \tag{3.17}$$

where $\tilde{K}_{\text{ave}}$ and $\tilde{G}_{\text{ave}}$ are the bulk and shear moduli of a homogeneous mixture with concentration c_{ave}, K' and G' are constants, and ϕ is related to the concentration c by (3.8). That is, the elastic moduli vary linearly with concentration near the initial state.

In the process of aggregation during which phase separation into precipitate, matrix, and interface regions is underway, at any instant in time there will be material points with concentrations distinct from c_{m} or c_{p}. Therefore, estimates of elastic properties for continuum material points at any solute concentration are required to . The following observations are consistent with the simulations presented in Sec. 5-7: i) In well coarsened states, the interfacial region generally is characterized by $c_{\text{m}} \le c \le c_{\text{p}}$; ii) Regions surrounding a precipitate and its interface at concentrations $c \neq c_{\text{m}}$ exist during earlier stages of aggregation; and iii) Within precipitates $c \approx c_{\text{p}}$ throughout the process. Let $\left(K_{\text{m}}, G_{\text{m}}\right)$ and $\left(K_{\text{p}}, G_{\text{p}}\right)$ denote bulk and shear moduli of ideal matrix and precipitate material, respectively; each these moduli are assumed to be positive. For all material points at any local effective elastic moduli are assumed to lie within Voigt and Reuss bounds:

$$\begin{aligned} \left[\phi K_{\text{p}}^{-1} + \left(1-\phi\right) K_{\text{m}}^{-1}\right]^{-1} \le\ & \tilde{K}\ \le \phi K_{\text{p}} + \left(1-\phi\right) K_{\text{m}} \\ \left[\phi G_{\text{m}}^{-1} + \left(1-\phi\right) G_{\text{m}}^{-1}\right]^{-1} \le\ & \tilde{G}\ \le \phi G_{\text{p}} + \left(1-\phi\right) G_{\text{m}} \end{aligned} \quad . \tag{3.18}$$

Since the variations in moduli near the initial state (3.17) and the Voigt upper bound are both linear in ϕ, for simplicity adopt the Voigt estimates (3.18) for the bulk and shear moduli as a function of concentration. For the numerical simulations presented below, at any state in the

aggregation process the effective elastic moduli are taken to be a linear function of $\phi(\mathbf{x},t)$:

$$\begin{aligned} \tilde{K} &= \phi K_{\mathrm{p}} + (1-\phi) K_{\mathrm{m}} \\ \tilde{G} &= \phi G_{\mathrm{p}} + (1-\phi) G_{\mathrm{m}} \end{aligned} \quad . \tag{3.19}$$

4 Numerical analysis

The non-equilibrium aggregation process is governed by the diffusion equation (2.4) associated with a monotonic decrease of free energy comprising chemical, interfacial, and elastic energies, where the latter is coupled to solutions to the Navier equation (2.8). The chemical energy is modeled by a Ginzburg-Landau type polynomial (3.5); the interfacial energy is associated with concentration gradients, ∇c, i.e. the second term in (2.1); and the elastic energy is given by (2.6) and depends upon the transformation strain and elastically heterogeneity.

The coupled equations (2.4) and (2.8) are solved numerically in non-dimensional form:

$$\frac{\partial \phi}{\partial \hat{t}} = \hat{\nabla}^2 \left[\phi(\phi-1)(2\phi-1) - \hat{\nabla}^2 \phi + \frac{\partial \hat{E}(\phi, u_i)}{\partial \phi} \right] , \tag{4.1}$$

$$\left\{ \hat{C}_{ijkl} \left[\frac{1}{2}\left(u_{k,l} + u_{l,k}\right) - \varepsilon_{kl}^{\mathrm{T}} \right] \right\}_{,j} = 0 \ , \tag{4.2}$$

where $\hat{x}$, $\hat{t}$, $\hat{C}_{ijkl}$ are dimensionless length, time, and effective moduli, respectively, given by

$$\hat{x} = x/\delta_{\mathrm{o}} , \quad \hat{t} = \frac{t\,\delta_{\mathrm{o}}^2}{2M\, w_{\mathrm{o}} \left(c_{\mathrm{p}} - c_{\mathrm{m}}\right)^2}, \quad \text{and} \quad \hat{C}_{ijkl} = \frac{\tilde{C}_{ijkl}}{2w_{\mathrm{o}} \left(c_{\mathrm{p}} - c_{\mathrm{m}}\right)^2} \ , \tag{4.3}$$

where the only length scale entering the governing equations is

$$\delta_{\mathrm{o}} = \sqrt{\gamma / w_{\mathrm{o}}} \left(c_{\mathrm{p}} - c_{\mathrm{m}}\right)^{-1} \ . \tag{4.4}$$

Wheeler et al. (1992) show that the thickness of the interface for a 1D Cahn-Hilliard problem with the Ginzburg-Landau potential (3.5) is on the order of δ_{o}, which varies from nanometers to

ten nanometers for metal alloys. As δ_o decreases, gradients of concentration in the interface increase and, consequently, contributions from gradients of elastic properties to the Navier equation (2.8) become more important. Note that the material parameters w_o, γ, c_p and c_m do not appear explicitly in the in the dimensionless equations (4.1) and (4.2), and at most only five parameters need to be specified: the transformation strain, ε^T, and $\hat{K}_m, \hat{G}_m, \hat{K}_p, \hat{G}_p$, the moduli normalized by $2w_o\left(c_p - c_m\right)^2$. In the following, we take Poisson's ratio to be the same in each phase and, therefore, the number of parameters to be specified reduces to four. Furthermore, with the Voigt estimates for $\tilde{K}$ and $\tilde{G}$, $\tilde{\nu} = \nu_p = \nu_m$. For metal alloys such as Cu-Ag or Ni-Al (Vaithyanathan and Chen, 2002) at temperatures in the range 500-1000 ^oK, w_o is approximately on the order of $10^9 - 10^{10}\ J/m^3$ and the dimensionless bulk modulus, from (4.3), is on the order of 50 to 500. The magnitude of transformation strain, ε^T, ranges from a fraction of a percent to several percent or even larger, although a large transformation strain likely would involve inelastic deformation which is not consider in this work.

The non-linear PDEs (4.1) and (4.2) are solved numerically for 2D problems using finite differences. These equations of mass transport and mechanical equilibrium are coupled. However, since the elastic response is rate independent, i.e. instantaneous and, therefore, in essence much faster than diffusion, the system must always be in force equilibrium. Explicit time-integration of (4.1) leads to a numerical algorithm in which the governing equations are solved sequentially, albeit with generally small time steps. Given a concentration field, $c\left(x, y, t\right)$, the heterogeneous elasticity problem (4.2) is solved to obtain the mechanical fields at time *t*. Then, from the corresponding estimate of elastic energy field at time *t*, the concentration

distribution for the next time step, $c(x, y, t+\Delta t)$, is calculated from the diffusion equation (4.1).

For the domains and boundary conditions of the problems considered below, a regular grid (square mesh) is adopted. The grid spacing is taken to be about one fourth of the thickness of the interface to ensure accuracy of the simulations.

The calculation the displacement field for each time increment is the most time consuming part of the simulation. The system of linear equations resulting from the discretization of (4.2) can be solved either by a direct method, such as LU decomposition, or an iterative method, such as Gauss-Seidel. For small time increments, the iterative method tends to be more efficient, since the solution from a previous increment is a good initial guess for the updated displacement field. The Bi-Conjugate Gradients Stabilized method (BICGSTAB) developed by Van Der Vorst (1992) is used to solve the linear equations for displacement field. The overall efficiency is improved further by factors of two to five using the successive over-relaxation method (SOR) as a preconditioner, which also has been incorporated (Van Der Vorst, 1992).

The time increment in explicit integration generally has to be very small to maintain stability. For an aggregation problem associated with a monotonic decrease in free energy, a constant time increment is inefficient. A self-adaptive, time-stepping algorithm is used in this work. At each grid point (x_i, y_j), the discrete form of (4.1) can be expressed as

$$\phi_{ij}^{n+1} - \phi_{ij}^{n} = \Delta t \, g_{ij}^{n} \quad , \tag{4.5}$$

where g_{ij}^{n} represent the numerical value of right-hand side of (4.1). For stability the time increment is chosen to be

$$\Delta t = \frac{\varsigma}{\left| g_{ij}^{n} \right|_{\max}} \quad , \tag{4.6}$$

where ς is a constant taken to be 0.005 for the results presented in this paper. As equilibrium is approached, the magnitude of the driving force, $\left| g_{ij}^{n} \right|$, tends to decrease and, therefore, the allowable time increment tends to steadily increase. For the simulations presented below, the average time increment is approximately an order of magnitude larger than the initial time increment.

5 Aggregation in the bulk

To begin our systematic study of the effects of compositionally-dependent elastic properties and transformation strain on aggregation, in this section we consider bulk aggregation, with complete solutions to the Navier equations for generally heterogeneous media. Overall coarsening evolves as the total energy of the system decreases, as one would expect. These simulations motivate a detailed investigation in Sec. 6 of elastic energies in composite systems undergoing transformations, including a study of an idealized 2-particle problem to demonstrate correlations between those effects and estimates of self and interaction energies.

For the bulk aggregation problem, a two-dimensional square domain is considered with periodic boundary conditions on both the mass transport and the displacement fields. The initial condition is given by

$$\phi(x, y, 0) = \phi_{\text{ave}} + \xi(x, y) \quad , \tag{5.1}$$

where $\phi_{\text{ave}} = (c_{\text{ave}} - c_{\text{m}}) / (c_{\text{p}} - c_{\text{m}})$ and $\xi(x, y)$ represents small fluctuations about that value; for all results presented in this paper, $\phi_{\text{ave}} = 0.25$. The random fluctuation $\xi(x, y)$ are taken

to have a normal distribution in the range $[-0.001,\ 0.001]$. To ensure good statistics, the size of the domain must be large enough to accommodate many, e.g. hundreds, of precipitates. The grid spacing is taken to be on the order of 1/4 of the interface thickness, which is approximately $8\delta_{\mathrm{o}}$ (see eq. 4.4). The simulation cell is a 512×512 square grid (appoximately 1024x1024 δ_{o}). For all results in this paper, the dimensionless bulk modulus of matrix $\hat{K}_{\mathrm{m}}=100$, which is typical of metal alloys, and Poisson's ratios are taken to be $\nu_{\mathrm{m}}=\nu_{\mathrm{p}}=0.3$. Various magnitudes of transformation strain, ε^{T}, and contrast κ in bulk moduli between matrix ($\phi=0$) and precipitate ($\phi=1$) phases are considered, where,

$$\kappa\equiv\hat{K}_{\mathrm{p}}\big/\hat{K}_{\mathrm{m}}\quad .$$

We begin with $\varepsilon^{\mathrm{T}}=0.005$ and $\kappa=1$. Representative morphologies at short, intermediate, and long times in the aggregation process are depicted in Fig. 2 a-c, respectively. In Fig.2 (and other graphics presented below), the deepest blues represents the regions that are depleted of solute, and red represents the precipitate phase. Phase separation evolves from the initial, nearly uniform concentration field, i.e. specified by (5.1) with $\phi_{\mathrm{ave}}=0.25$, followed by stages of growth and coalescence. Average energy densities – total, chemical, interfacial, and elastic – as a function of time are plotted in Fig. 3, with the longest times corresponding to the morphology in Fig. 2c. The individual contributions to the total energy are computed from spatial integrals of the three terms, respectively, on the right-hand side of (2.1). The normalized time is defined in (4.3), and all energies are normalized by $2w_{\mathrm{o}}\left(c_{\mathrm{p}}-c_{\mathrm{m}}\right)^2$.

The portion of the total energy associated with interfacial energy, i.e. the spatial integral of $\gamma\nabla c\cdot\nabla c$ (with major contributions from interfacial regions) depends on several material properties

including Γ_{int}, as discussed in Sec. 3.2,. Coarsening is clearly seen to be associated with a monotonic decease of total energy due, primarily, to a reduction in total interfacial area (in 2D). This reduction requires that material previously in the interfacial region, which is at intermediate concentrations between the matrix and precipitate values, be continuously redistributed to precipitate and matrix regions in order to keep the total concentration fixed. As a result, the total chemical energy also decreases and, as predicted in these simulations, the total elastic energy slightly increases as the system coarsens. This slight increase in elastic energy is likely due to higher elastic energy in the precipitate region than in the interfacial region, consistent with the rule for the transformation strain (3.13), but its dependence on the evolution of the heterogeneous elasticity problem, (2.8), is certainly complex. Nevertheless, in this case ($\varepsilon^{\text{T}} = 0.005$ and $\kappa = 1$), the elastic energy is small compared to the chemical and interface energies that tend to roughly equal values.

For other values of ε^{T} and κ morphologies similar to those in Fig. 2 are predicted, while the evolution of energies and, therefore, kinetics of aggregation are affected. As the magnitude of the transformation strain increases, the total elastic energy tends to increase, but its magnitude depends upon the elastic contrast as discussed in Sec. 6.

A measure of the overall kinetics is the evolution of the average radius of precipitates $\hat{R} = R/\delta_{\text{o}}$. Given that the interface between precipitate ($\phi = 1$) and matrix ($\phi = 0$) is relatively thin, the size of precipitate is defined to be the region where $\phi \geq 0.5$ (as in Eggleston et al., 2001). For the case of homogeneous elastic properties, $\kappa = 1$, $\hat{R}$ vs. *t* kinetics are plotted in Fig. 4 for various ε^{T}, where the same initial fluctuations are applied in each case and the longest times in these

simulations correspond to morphologies like Fig. 2c. The rate of aggregation is shown to increase with increasing magnitude of transformation strain, essentially due to an increase in the magnitude of gradients of elastic energy density, and is found to be nearly independent of the sign of the transformation strain. These observations are consistent with simple estimates of self and interaction energies introduced in Sec. 6.2.

Systems with inhomogeneous elastic properties are considered next. The $\hat{R}$ vs. t system kinetics for $\kappa = \frac{1}{2}$, 1, and 2 are plotted in Fig. 5 for a transformation strain of $\varepsilon^{\mathrm{T}} = 0.005$. Compared to the homogeneous case ($\kappa = 1$), on the average aggregation is slightly faster for systems with stiffer precipitates and slower for softer precipitates. In both cases the coarsening rates are faster than without the effects of elastic energy ($\varepsilon^{\mathrm{T}} = 0$). These findings also are consistent with theoretical considerations of self and interaction energies and further support the notion that gradients in elastic energy density promote coarsening. Hu and Chen (2001) consider systems with different shear but identical bulk moduli, and their findings are qualitatively different, probably due to the fact that they considered only a very high volume fraction $\phi_{\mathrm{ave}} = 0.5$ which does not lead to well defined precipitates (inclusions).

Figures 4 and 5 clearly demonstrate that the kinetics of aggregation depends non-trivially on the non-uniform elastic fields arising from both the intrinsic transformation strain and elastic heterogeneity (contrast). Detailed analyses of the simulations, which for brevity is not presented, show that increasing the magnitude of the transformation strain generally has the effect of increasing the non-uniformity in the elastic fields for a given contrast in elastic properties. For a positive transformation strain, the non-uniformity in the elastic fields

increases with increasing stiffness of the precipitate and decreases for decreasing stiffness; for a negative transformation strain the trends are similar. These are somewhat intuitive findings. The corresponding effects on the average magnitudes of the driving forces for aggregation are less obvious, but in general the greater the driving force the faster the aggregation. These observations also are consistent with simple estimates of self and interaction energies introduced in Sec. 6.2.

6. Elastic Energies

The magnitude of the transformation strain as well as elastic heterogeneity have a direct effect on the kinetics of coarsening in the bulk, as seen in Figs. 4 and 5. These trends are interpreted in this section utilizing Eshelby's ideas on self energy and interaction energies between precipitates and with external loads. (see Eshelby 1957; Ardell and Nicholson, 1966; Eshelby, 1966; Mura, 1982). In general, analytical estimates for these energies are limited to dilute concentrations and small contrast in elastic heterogeneity, but somewhat unexpectedly they are rather reliable even well beyond of those limits. In the absence of external load, there is direct correlation between the magnitude of the total elastic energy in an aggregating system and the magnitude of non-uniformity of elastic energy, which in turn tends to increase the magnitude of mass flux. This is demonstrated both for the bulk aggregation problem and for an idealized two-precipitate system. In addition, estimates for interaction energies that arise from external load are developed at the end of this section (and shown, in Sec. 7, to correlate well with the thin film simulations).

6.1 Elastic energy without external load

Consider a system with N (non-overlapping) heterogeneous and dilating (transforming) ellipsoidal precipitates. The total elastic energy can be partitioned as (Eshelby, 1966):

$$E_{\text{tot}} = E_{\text{self}} + E_{\text{int}} = \sum_{i=1}^{N} E_i + \sum_{i \neq j=1}^{N} E_{ij} + \ldots \quad , \tag{6.1}$$

where the first term in the right hand side of (6.1) represents of the self energy associated with each precipitate of distinct elastic properties taken individually in a homogenous matrix and the second term is the additional energy due to the interaction between precipitates. Here we consider only two-body interactions. In the absence of external loading, E_{tot} represents the term $E(\boldsymbol{\varepsilon}, c)$ in the free energy (2.1). Elastic effects have a direct influence on the rate of coarsening as shown from simulations of bulk aggregation (see, Figs. 4 and 5). The redistribution of solute in the system is driven by the non-uniformity of the free energy, and the driving force tends to increase with the increasing E_{tot}, i.e. for a given morphology the higher energy generally implies higher energy gradients.

Self and interaction energies as a function of ε^{T} and κ can be estimated using Eshelby's ideas for both dilute concentration ($c \ll 1$) and small elastic contrast ($\kappa \approx 1$). Below we give explicit results for cylindrical precipitates undergoing dilational transformations, i.e. $\varepsilon_{11}^{\text{T}} = \varepsilon_{22}^{\text{T}} = \varepsilon^{\text{T}}$, which are needed for comparisons to our 2D simulations (Eshelby, 1961 and 1966, and Johnson, 1984, considered the analogous problems for spheres). Eshelby (1961) demonstrated that E_{int} in (6.1) vanishes for homogeneous and isotropic systems under dilational transformations in the absence of externally applied loads. The derivation of the self and

interaction energies is given in the Appendix, and the results are summarized below.

For N=2, (6.1) is written as:

$$E_{\text{tot}} = E_1 + E_2 + E_{12} \quad . \tag{6.2}$$

For a precipitate in an infinite body undergoing a dilational transformation, the axisymmetric radial displacement field is linear in the radial coordinate inside the dilating cylinder and of the form $c_1 r + c_2 / r$ outside. With r_1 and r_2 denoting the radii of two non-overlapping precipitates, the self energies can be expressed as:

$$E_1 + E_2 = \alpha\left(r_1^2 + r_2^2\right) \quad . \tag{6.3}$$

With small elastic contrast and for $\nu_{\text{p}} = \nu_{\text{m}} = \nu$, which is adopted for all simulations presented in this paper, a straightforward analysis that follows Eshelby (1966) yields:

$$\alpha = \lambda\left(1-2\nu\right)\left(\varepsilon^{\text{T}}\right)^2 \kappa \quad , \tag{6.4}$$

where ,

$$\lambda = \frac{3\pi\left(1-2\nu\right)K_{\text{m}}}{4\left(1-\nu\right)^2\left(1+\nu\right)} \quad .$$

Therefore, the self energy for two precipitates is positive, quadratic in the magnitude of transformation strain, and proportional to κ for $\nu_{\text{p}} = \nu_{\text{m}} = \nu$. This result generalizes immediately for N precipitates.

For small elastic contrast and in the dilute limit, the two-particle interaction energy is:

$$E_{12} = E_{\text{int}} = \beta r_1^2 r_2^2 \left[\frac{r_1^2}{\left(d^2 - r_2^2\right)^2} + \frac{r_2^2}{\left(d^2 - r_1^2\right)^2}\right] \quad , \tag{6.5}$$

where d is the distance between the centers of the precipitates and β is given by:

$$\beta = \lambda \left(\varepsilon^{\mathrm{T}} \right)^2 (\kappa - 1) \quad . \tag{6.6}$$

From (6.5) and (6.6) we see that the interaction energy between precipitates is also quadratic in ε^{T}, it vanishes for $\kappa = 1$, is positive for $\kappa > 1$, and is negative for $\kappa < 1$. Again, in the dilute limit, the interaction energy is readily extended for N precipitates. Estimates in the non-dilute limit, which would require extensive numerical analyses, are not available.

For an elastically homogeneous and dilute system, the total elastic energy (and self energy since $\kappa = 1$) is quadratic in the magnitude of transformation strain and, therefore, independent of the sign of the transformation strain. Consequently, the elastic energy monotonically increases with the magnitude of transformation strain. For a given morphology and some ϕ_{ave}, an increase in elastic energy tends to correspond to an increase in the non-uniformity of the chemical potential and, as a result, increase the average magnitude of the mass flux, or equivalently, the so-called apparent diffusion coefficient (Larche and Cahn, 1982). Therefore, coarsening is relatively faster in a system with greater magnitude of transformation strain as seen in Fig. 4; for example, at a given $\hat{R}$, which roughly corresponds to similar morphologies, the rate of coarsening, $\mathrm{d}\hat{R}/\mathrm{d}t$, increases with ε^{T}.

For an elastically heterogeneous system, the interaction energy, E_{int}, in (6.1) is positive for stiffer precipitates and negative for softer precipitates as given in (6.5) with (6.6). Relative to the homogeneous case, a system with $\kappa < 1$ is energetically more stable (favorable) due to the negative interaction energy, and consequently, the coarsening rate is slower than in an elastically homogeneous ($\kappa = 1$) system. Similarly, one can draw the conclusion that the coarsening rate tends to increase for $\kappa > 1$ since the interaction energy is positive. Simulations for bulk

aggregation (Figs. 4 and 5) (as well as the two particle systems discussed in Sec. 6.2) are consistent with these trends. In an investigation of Ostwald ripening using a sharp interface model, Kawasaki and Enomoto (1988) assume dependencies of the velocity of interfaces on the interaction energy that are consistent with (and justified by) these findings.

6.2 Coarsening in a two-particle system

To further demonstrate the ideas in Sec 6.1, we investigate an ideal system derived from two representative neighboring precipitates that were extracted from the morphology of Fig. 2a and embedded into a homogeneous matrix as shown in Fig. 6a. Given this initial distribution $c(\mathbf{x},0)$, the corresponding distributions of $\boldsymbol{\varepsilon}^{\mathrm{T}}(\mathbf{x},0)$ and $\tilde{\mathbf{C}}(\mathbf{x},0)$ are also imposed according to the constitutive equations in Sec. 3. With only two precipitates, a square domain with a 128×128 mesh is sufficient, again with the mesh size chosen to be about one forth of the interface thickness. For this ideal initial configuration, coarsening causes the larger precipitate to grow at the expense of the smaller one, as seen in the representative morphologies of Fig. 6. The kinetics of this process can be measured by the evolution of the radius of the smaller particle, which is plotted in Fig. 7 for various combinations of ε^{T} and κ. The variations in the coarsening rates with various ε^{T} and κ are completely consistent with the theoretical considerations discussed in Sec. 6.1: i) for fixed κ, coarsening accelerates as $\left|\varepsilon^{\mathrm{T}}\right|$ increases and ii) for fixed ε^{T}, coarsening accelerates as $\kappa \equiv K_{\mathrm{p}}/K_{\mathrm{m}}$ increases. As in the case of bulk aggregation, for this two-particle system the magnitude of the mass flux tends to increase with increasing the total elastic energy, which is always positive, while the contribution for the interaction energy can be positive or negative.

6.3 Interaction between external load and precipitates

As noted above, in Sec. 7 aggregation in a thin film under patterned external load is studied in detail. In addition to the elastic energies discussed in Sec. 6.1, the interaction energy associated with external tractions and (internal) transformation strain becomes important; related ideas are considered in Mura (1982) in isotropic and anisotropic solids under remote tractions corresponding to a uniform stress state. In an elastically homogeneous system containing a dilute concentration of ellipsoidal precipitates (both Eshelby and Mura refer to these as inclusions in the homogeneous case), with cylinders a special case, the interaction energy is given by:

$$E_{\text{int}}^{\text{o}} = -V\sigma_{ij}^{\text{o}}\varepsilon_{ij}^{\text{T}} \quad , \tag{6.7}$$

where σ_{ij}^{o} is a uniform stress field that defines the traction $T_i = \sigma_{ij}^{\text{o}} n_j$, where n_j is the outward normal to some remote boundary, and V is the total volume of precipitates undergoing a transformation strain $\varepsilon_{ij}^{\text{T}}$. For dilational transformations, $\varepsilon_{ij}^{\text{T}} = \varepsilon^{\text{T}}\delta_{ij}$ ($i, j = 1,2$), the interaction energy is simply

$$E_{\text{int}}^{\text{o}} = -V\sigma_{kk}^{\text{o}}\varepsilon^{\text{T}} \quad , \tag{6.8}$$

Consequently, the interaction energy is negative for dilatational precipitates ($\varepsilon^{\text{T}} > 0$) in tensile regions and for contractional precipitates ($\varepsilon^{\text{T}} < 0$) in compressive regions. In opposite cases, the interaction energies are positive. Therefore, precipitates undergoing concentration-dependent dilational or contractional transformation strains, i.e. (3.12), are expected to be energetically favored in locally tensile or compressive regions, respectively.

For the elastically heterogeneous system, precipitates are commonly referred to as

inhomogeneities. Eshelby (1957) pointed out that the stress disturbance of an inhomogeneity due to an applied uniform traction is equivalent to that of an inclusion (with same elastic properties as matrix) with an appropriately chosen transformation strain, ε_{ij}^{*}. For an axisymmetric external load i.e., $\sigma_{ij}^{\mathrm{o}} = \sigma^{\mathrm{o}}\delta_{ij}$ $(i, j = 1,2)$, the corresponding transformation strain for a cylindrical precipitate in an infinite matrix is:

$$\varepsilon_{ij}^{*} = \frac{2\left(1-\nu^{2}\right)\left(1-\kappa\right)}{3K^{\mathrm{m}}\left(\kappa+1-2\nu\right)}\sigma^{\mathrm{o}}\delta_{ij} \quad . \tag{6.9}$$

The derivation of this equation is straightforward (with $u_r = c_1 r$ in precipitate and $u_r = c_2 r + c_3/r$ in matrix) and will not be given here. In this case, following Mura (1984, Sec. 25), the interaction energy is given by (6.7) with $\varepsilon_{ij}^{\mathrm{T}} = \varepsilon_{ij}^{*}$ plus the additional term $\frac{1}{2}V\sigma_{ij}^{\mathrm{o}}\varepsilon_{ij}^{*}$. Therefore, for the heterogeneous system in the absence of transformation strain ($\varepsilon^{\mathrm{T}} = 0$), the interaction energy is:

$$E_{\mathrm{int}}^{\mathrm{o}} = -\frac{V}{2}\sigma_{ij}^{\mathrm{o}}\varepsilon_{ij}^{*} = \frac{V\left(1-\nu^{2}\right)\left(\kappa-1\right)}{6K^{\mathrm{m}}\left(\kappa+1-2\nu\right)}\left(\sigma_{kk}^{\mathrm{o}}\right)^{2} \quad , \tag{6.10}$$

i.e., e_{int} is positive for stiffer precipitates ($\kappa > 1$) and negative for softer precipitates ($\kappa < 1$). Therefore, for remote axisymmetric stressing, the interaction energy is lower for stiffer precipitates forming in lower stressed regions and for softer precipitates forming in higher stressed regions. The (total) interaction between the precipitate and applied stress for heterogeneous systems is the sum of (6.8) and (6.10); note that the dependence on load is linear in coupling with the transformation strain and quadratic but normalized by the bulk modulus in coupling with elastic contrast. Under more general states of stress, similar dependencies on its magnitude and on the elastic contrast are anticipated and demonstrated in relation to the

morphologies predicted in thin film simulations presented in the next section.

In summary, due to a uniformly applied remote traction, the interaction energy for dilating precipitates in elastically homogeneous systems is estimated (for dilute concentrations) to be proportional to σ^{o}_{kk} and negative if ε^{T} and σ^{o}_{kk} have the same sign. For heterogeneous precipitates (for dilute and small contrast) there is an additional contribution to the interaction energy given by (6.10), which is quadratic in σ^{o}_{kk}, positive for $\kappa > 1$, and negative for $\kappa < 1$. The observed kinetics and morphology for aggregation in thin films under non-uniform tractions presented in the next section are interpreted using the estimates (6.8) and (6.10) by associating the local stresses arising in the film in the regions surrounding a precipitate with the remote stress σ^{o}_{ij} entering those estimates. Precipitates with $\varepsilon^{T} \neq 0$ and $\kappa = 1$ tend to aggregate in regions where σ_{kk} and ε^{T} have the same sign, and where σ_{kk} is maximum for $\varepsilon^{T} > 0$ or minimum for $\varepsilon^{T} < 0$. For $\varepsilon^{T} = 0$, precipitates are energetically favored in regions of high σ_{kk} for $\kappa < 1$ or low σ_{kk} for $\kappa > 1$.

7 Aggregation in a thin film under external load

From simulations of aggregation in the bulk, intrinsic elastic effects have been shown to directly affect the kinetics of coarsening, with self and interaction energies between precipitates playing a significant role. Next, we consider the effects of non-uniformly imposed external load (tractions) on aggregation in thin films. The objective is to demonstrate that elastic interactions arising from patterned tractions, which also affect kinetics, can be used to control the morphology of aggregation, i.e., the microstructure.

Consider a film with a nearly uniform initial state that is loaded by normal tractions, which approximate indentation by a circular cylinder (2D). We consider both a single indenter and, in the majority of simulations, periodically-arranged distributions of tractions. In the periodic case, the film of dimension $L \times H$ is loaded as depicted in Fig. 8. For simplicity, a Hertz-type contact traction distribution (e.g., for a rigid cylinder on a half-space) is assumed for each indentor:

$$\sigma_{yy}\left(x, \pm H/2, t\right) \equiv P\left(x\right) = \begin{cases} P_{\max}\left(1 - x^2/a^2\right) & x \in \left[-a, a\right] \\ 0 & x \in \left[-b+a, b-a\right] \end{cases}, \tag{7.1}$$

where $2b$ is the spacing between indenters of width $2a$, $P_{\max}$ is the maximum magnitude of stress, and the origin of the x coordinate is located at the symmetry line of any one of the distributions. For all of the simulations presented below the normalized magnitude $\hat{P}_{\max} = P_{\max} \Big/ \left[2w_{\mathrm{o}} \left(c_{\mathrm{p}} - c_{\mathrm{m}} \right)^2 \right]$ is taken to be -0.5 (compressive), which corresponds to $P_{\max}$ on the order of 10-500 MPa for metal alloys (based upon typical values of w_{o}, c_{m} and c_{p} cited above). The first set of results are for the thinner film ($\hat{H} \equiv H/\delta_{\mathrm{o}} = 8$) compressed by single indenter; the second set of results are for a film that is 8 times thicker ($\hat{H} = 64$) with a unit cell containing four equally-spaced indenters to account for statistical variations (see Fig. 8). For both cases zero mass-flux condition is applied on the top and bottom surfaces and periodic conditions on mass transfer on the left and right ends. The top and bottom surfaces are loaded by normal traction distributions of the form (7.1) with zero shear traction, while periodic conditions on displacement are applied on left and right sides. Initial concentrations are given

by (5.1).

7.1 Single indenter

Consider a single indenter applied on the film with dimensions $\hat{H} = 8$, $L/H = 32$ and $a/H = 2$. The film is chosen to be sufficient thin so that, as equilibrium is approached, the precipitates tend to span the thickness dimension. As in the previous simulations, $\hat{K}_{\mathrm{m}} = 100$ and $\nu_{\mathrm{p}} = \nu_{\mathrm{m}} = 0.3$, while ε^{T} and κ are varied. The mean stress (negative pressure), $\sigma_{kk}/3$, due to the applied tractions (7.1) acting on an elastically homogeneous film in the absence of transformation strain is plotted in Fig. 9. The magnitude of hydrostatic mean stress is greatest beneath the indenter, while the region far away from the indenter is essentially stress free. A small tensile region initially exists adjacent to the indentors, which does influence aggregation in some cases. The corresponding short-time precipitation (for $\kappa = 1$ and $\varepsilon^{\mathrm{T}} = 0$) is random, as seen in Fig. 10a. In this case, external load has no effect on the concentration field, since there is no coupling, i.e., the interaction energy is identically zero. With $c \approx c_{\mathrm{ave}}$ everywhere, the initial stress distributions are similar for other cases, i.e. with $\varepsilon^{\mathrm{T}} \neq 0$ and/or $\kappa \neq 1$, while, in general, σ_{kk} changes during aggregation due to elastic interactions which affect the kinetics and morphology of precipitation.

For $\varepsilon^{\mathrm{T}} \neq 0$ and/or $\kappa \neq 1$, precipitation under non-uniform load is no longer random. The external load directly affects the location of precipitates as seen in Figs. 10b-e. Precipitates are: i) adjacent to the indenter, i.e., outside of the high compression region for films with $\varepsilon^{\mathrm{T}} > 0$ and $\kappa = 1$ or $\varepsilon^{\mathrm{T}} = 0$ and $\kappa > 1$ or ii) beneath the indenter in the high compression region, for films

with $\varepsilon^{\mathrm{T}} < 0$ and $\kappa = 1$ or $\varepsilon^{\mathrm{T}} = 0$ and $\kappa < 1$.

The morphologies shown in Figs. 10b-e can be correlated with interaction energies if the stress σ_{ij}^{o} entering (6.8) and (6.10) are interpreted as the local stress that exists initially in the loaded state (see Fig. 9). In the case of elastically homogeneous systems, dilating precipitates tend to form in tensile regions (Fig. 10b), and contracting precipitates tend to form in compressive regions (Fig. 10c), where in both cases the interaction energy estimated by (6.8) is negative. With elastic contrast in the absence of external load, from (6.10) one expects that softer precipitates are energetically favored in the highest stressed regions under the indenter, which is consistent with Fig. 10e. Stiffer precipitates tend to form in lower stressed regions, and since the region under the indenter is energetically unfavorable, the solute diffusing from that region tends to aggregate just outside of the indenter as seen in Fig 10d. For other combinations of ε^{T} and κ, morphologies are also consistent with trends predicted from (6.8) and (6.10) are predicted, but details are left for a subsequent paper.

7.2 Periodic indentation

Next, we consider periodically applied stress as depicted in Fig. 8 on a thicker film ($\hat{H} = 64$ and $L/H = 32$), which allow several precipitates to form through the thickness. In order to introduce non-trivial statistics the unit cell is taken to have four loading periods, each represented by (7.1) with $a = H = b/2$. The initial stress distribution under the indentor is similar to Fig. 9. Representative states of aggregation for the films with various ε^{T} and κ at short, intermediate, and long times are depicted in Figs. 11-14.

i) In elastically homogeneous systems with transformation strain ($\varepsilon^{\mathrm{T}} \neq 0$ and $\kappa = 1$), nearly periodic patterns emerge during early stages of aggregation due to strong coupling between stress and transformation strains: a) for dilational transformations, the precipitates preferentially form at the edges of the indenters (regions with small, initial tensile stress) as seen in Figs. 11a and 11b; b) for contractional transformations the precipitates preferentially form beneath the indenters as seen in Figs. 12a and 12b. In both cases, the interaction energy between external load and transformation strain is estimated to be minimum in these regions if we interpret σ_{ij}^{o} in (6.8) as the local stress in the film. Furthermore, by comparing the contrast between light blue (corresponding roughly to c_{ave} or $\phi_{\mathrm{ave}} = 0.25$) and darker blue (corresponding roughly to c_{m} or $\phi = 0$) regions, e.g., in Figs. 11b and 12b, one sees that precipitation tends to be faster in regions with higher elastic energy density, i.e., below and adjacent to the indenter, than that in regions between the indenters, i.e., nearly unstressed regions.

The morphologies for intermediate times evolve from those short-time distributions as precipitates coarsen and coalesce: see Figs 11c, d and 12c, d. For $\varepsilon^{\mathrm{T}} > 0$ and $\kappa = 1$, the precipitates tend to grow near the edge of the indenters, drawing solute from both underneath and between the indenters, as seen in Fig. 11e. For $\varepsilon^{\mathrm{T}} < 0$ and $\kappa = 1$, one relatively large precipitate aggregates beneath each indenter as seen in Fig. 12e. In the homogeneous system, equilibrium configurations are attained more quickly for dilatational precipitates than contractional ones. This observation is consistent with the fact that the interaction energy (6.8) in the latter case is more negative than in the former one, which tends to reduce the driving force for diffusion. Therefore, elastic effects that decrease/increase the total energy during

aggregation (intermediate times) relative to the long-time energy tend to decrease/increase the rate of aggregation.

The morphologies shown in Figs. 11e and 12e persist for much longer times (beyond $\hat{t} \approx 40,000$). This is not surprising, since the precipitates extend across the thickness in elastically-favored regions and, therefore, the interfacial energy cannot be reduced further unless they coalesce, which is not possible due to the effects of elastic interaction with the applied load. One final note for these cases ($\varepsilon^{\mathrm{T}} \neq 0$ and $\kappa = 1$): the intermediate and long-time morphologies for films are not sensitive to the initial fluctuations. This has been confirmed by varying the initial random distributions (5.1), which only affect the early stages of aggregation.

ii) For heterogeneous systems in the absence of transformation strain, the short-time morphologies tend to be more random, presumably due to the weaker elastic effects; note that the estimates of self energies (6.3) and precipitate-precipitate interaction energies (6.5) vanish in the dilute limit. Enhanced precipitation is observed adjacent to the indenters for stiffer precipitates (Fig. 13a) and beneath the indenters for softer precipitates (Fig. 14a). This is consistent with the effect of interaction energies between precipitates and applied stress (6.10); for $\varepsilon^{\mathrm{T}} = 0$ precipitation is favored in the low-stressed regions adjacent to indenter for $\kappa > 1$ (Figs 13b, c) and in the high-stressed regions below the indenter for $\kappa < 1$ (Figs. 14b, c). In both cases, the long-time morphologies (Figs. 13c and 14c) are effectively in equilibrium, which has been confirmed by extending the simulation beyond $\hat{t} = 10^6$. This is somewhat surprising since the interfacial energy would be further decreased if two precipitates coalesce through the thickness. However, complete coalescence seems to be suppressed by high elastic contrast. In these cases

($\varepsilon^{\mathrm{T}} = 0$ and $\kappa \neq 1$), short and long-time morphologies are found to be sensitive to the initial fluctuation. Simulations with eight different initial random fluctuations indicate that Figs. 13c and 14 c are the most probable long-time configurations. For $\kappa = 5$, two pairs of precipitates out of eight extended across the thickness in two out of eight simulations; for $\kappa = 1/5$, one pair of precipitates out of four extended across the thickness in one out of eight simulations. For brevity, those results are not presented. Nearly-periodic microstructures resulted in all simulations for long times.

8 Conclusions

A phase field model has been developed that includes spatially-varying elastic properties and coupling to an externally-imposed stress field. Constitutive relations have been adopted for the chemical energy, interfacial energy, transformation strain, and effective elastic moduli, all of which are key ingredients in the model. Two-dimensional simulations of aggregation in the bulk and in non-uniformly loaded thin films are in remarkably good agreement with theoretical considerations based upon estimates of the self and interaction energy of precipitates and the interaction energy between external load and precipitates, albeit in a dilute system with small elastic contrast. These estimates aid in the understanding of elastic effects and suggest how to control both the morphology and kinetics of aggregation through the application of patterned external loads.

Coarsening in the bulk tends to be faster as elastic energy increases, i.e., with increase in the magnitude of transformation strain and/or the stiffness of precipitates. Theoretical estimates of

the elastic energy are quadratic in the magnitude of transformation strain. Relative to an elastically homogeneous system, the elastic energy is higher for stiffer precipitates and lower for softer precipitates. Furthermore, an increase in the elastic energy tends to correspond to an increase in the magnitude of the mass flux and accelerates coarsening, which is further demonstrated through aggregation of a two-particle system.

Periodically patterned (non-uniform) external load is shown to be effective in guiding aggregation in thin films with non-zero transformation strain and/or elastic heterogeneity. Depending on the sign of the transformation strain, ε^{T}, and the magnitude of the contrast κ relative to the elastically homogeneous case, the precipitates tend to grow either adjacent to or beneath the indenter. These effects can be qualitatively interpreted via interaction energies between external load and precipitates, although the fields considered are more complex than those for which (6.8) and (6.10) are strictly valid. For example, soft precipitates tend to aggregate in highly stressed regions and contracting precipitates in regions of compressive, both of which exist under the indenter. Hard precipitates are favored in low-stressed regions and dilating precipitates in tensile regions, both of which exist adjacent to indenter. These findings have practical potential to guide the formation of patterned nano-structures.

Acknowledgements

The assistance of G.. Biros in developing the numerical algorithm, discussions with T. Sinno and E. Fried, and the support of the NSF/NIRT grant CTS 0404259 are gratefully acknowledged.

Appendix

The derivations for the self energy and the interaction energy between two precipitates, i.e.,

(6.3)-(6.6), are outlined below and follows Eshelby (1966) and Mura (1982).

The total elastic energy for a system of non-overlapping precipitates occupying a total volume V_{p} in an infinite matrix, each undergoing a transformation strain $\varepsilon_{ij}^{\mathrm{T}}$ in the absence of externally applied load, can be expressed as (Mura 1982):

$$E = \frac{1}{2}\int_{V} \sigma_{ij}\left(\varepsilon_{ij} - \varepsilon_{ij}^{\mathrm{T}}\right)dV = -\frac{1}{2}\int_{V_{\mathrm{p}}} \sigma_{ij}\varepsilon_{ij}^{\mathrm{T}}dV = E_{\mathrm{self}} + E_{\mathrm{int}} \quad , \tag{A.1}$$

where $\varepsilon_{ij} = \frac{1}{2}\left(u_{i,j} + u_{j,i}\right)$, E_{self} is the part of the energy associated with each precipitate transforming individually in an infinite homogeneous matrix, and E_{int} is the interaction energy between precipitates. Let variables with a prime denote an elastically heterogeneous system, i.e., $C_{ijkl}^{\mathrm{p}} \neq C_{ijkl}^{\mathrm{m}}$, and those without a prime a homogeneous system. In the absence of external load,

$$\int_{V_{\mathrm{p}}} \sigma_{ij}\varepsilon'_{ij}dV = \int_{V_{\mathrm{p}}} \sigma'_{ij}\varepsilon_{ij}dV = 0 \quad . \tag{A.2}$$

Therefore, for identical transformation strains in both systems, from (A.1) the total elastic energy of the heterogeneous system can be rewritten as:

$$E' = \frac{1}{2}\int_{V_{\mathrm{p}}} \sigma'_{ij}\left(\varepsilon_{ij} - \varepsilon_{ij}^{\mathrm{T}} - \varepsilon_{ij}\right)dV = \frac{1}{2}\int_{V_{\mathrm{p}}} \sigma'_{ij}\left(\varepsilon_{ij} - \varepsilon_{ij}^{\mathrm{T}}\right)dV \quad . \tag{A.3}$$

Similarly,

$$E = \frac{1}{2}\int_{V_{\mathrm{p}}} \sigma_{ij}\left(\varepsilon'_{ij} - \varepsilon_{ij}^{\mathrm{T}}\right)dV \quad . \tag{A.4}$$

Therefore, the variation of elastic energy due to elastic heterogeneity is given by:

$$\Delta E = E' - E = \frac{1}{2}\left(C_{ijkl}^{\mathrm{p}} - C_{ijkl}^{\mathrm{m}}\right)\int_{V_{\mathrm{p}}} \left(\varepsilon_{ij} - \varepsilon_{ij}^{\mathrm{T}}\right)\left(\varepsilon'_{kl} - \varepsilon_{kl}^{\mathrm{T}}\right)dV \tag{A.5}$$

For small elastic contrast, i.e., $C_{ijkl}^{\mathrm{p}} \approx C_{ijkl}^{\mathrm{m}}$, the difference in the primed and unprimed fields are

also small, and (A.5) can be approximated to first order in contrast by replacing ε'_{ij} with ε_{ij}, the strain field in the homogeneous system comprising of N precipitates, Consequently, ΔE can be partitioned as the change of self energy, ΔE_{self} and that of the interaction energy, ΔE_{int}, i.e.,

$$\Delta E_{\text{self}} = \sum_{\alpha=1}^{N} \frac{1}{2}\left(C^{\text{p}}_{ijkl} - C^{\text{m}}_{ijkl}\right) \int_{V_\alpha} \left(\varepsilon^{\alpha}_{ij} - \varepsilon^{\text{T}}_{ij}\right)\left(\varepsilon^{\alpha}_{kl} - \varepsilon^{\text{T}}_{kl}\right) dV \quad , \tag{A.6}$$

$$\Delta E_{\text{int}} = E_{\text{int}} = \sum_{\substack{\alpha,\beta=1 \\ \alpha\neq\beta}}^{N} \frac{1}{2}\left(C^{\text{p}}_{ijkl} - C^{\text{m}}_{ijkl}\right) \int_{V_\beta} \left[\left(\varepsilon^{\alpha}_{ij} - \varepsilon^{\text{T}}_{ij}\right)\left(\varepsilon^{\alpha}_{kl} - \varepsilon^{\text{T}}_{kl}\right) + 2\left(\varepsilon^{\alpha}_{ij} - \varepsilon^{\text{T}}_{ij}\right)\left(\varepsilon^{\beta}_{kl} - \varepsilon^{\text{T}}_{kl}\right)\right] dV \quad , \tag{A.7}$$

where $\varepsilon^{\alpha}_{ij}$ is the strain associated with precipitate α transforming in an infinite uniform matrix. Note that in the homogeneous dilute system, $E_{\text{int}} = 0$ (Eshelby, 1961).

Explicit results based upon the above relations are now obtained for an isotropic, cylindrical precipitate (2D) of radius r_{o} undergoing a dilational transformation, i.e., $\varepsilon^{\text{T}}_{ij} = \varepsilon^{\text{T}}\delta_{ij}$, in an unbounded matrix. Let K_{p}, G_{p} and ν_{p} denote the bulk modulus, shear modulus and Poisson's ratio, respectively, of the precipitate and K_{m}, G_{m} and ν_{m} the corresponding properties of the matrix. In this case and for an elastically homogeneous system,

$$\begin{aligned} \varepsilon_{\theta\theta} = \varepsilon_{rr} &= \frac{\varepsilon^{\text{T}}}{2\left(1-\nu_{\text{m}}\right)} && \text{for } r \le r_{\text{o}} \\ \varepsilon_{\theta\theta} = -\varepsilon_{rr} &= \frac{\varepsilon^{\text{T}}}{2\left(1-\nu_{\text{m}}\right)}\left(\frac{r_{\text{o}}}{r}\right)^2 && \text{for } r > r_{\text{o}} \end{aligned} \quad . \tag{A.8}$$

From (A.8), one sees that the strain field inside the precipitate is purely hydrostatic and uniform, while the strain field outside the precipitate is purely deviatoric (zero hydrostatic part). Consequently, ΔE_{self}, from (A.6)-(A.8), E_{self} and E_{int} in 2D can be expressed as:

$$E_{\text{self}} = \frac{\left(3K_p + G_P\right)\left(1-2\nu_{\text{m}}\right)^2}{6\left(1-\nu_{\text{m}}\right)^2}\left(\varepsilon^{\text{T}}\right)^2 \sum_{\alpha=1}^{N} \pi r_\alpha^2 \quad , \tag{A.9}$$

$$E_{\text{int}} = \frac{G_P - G_{\text{m}}}{2\left(1-\nu_{\text{m}}\right)^2}\left(\varepsilon^{\text{T}}\right)^2 \sum_{\substack{\alpha,\beta=1 \\ \alpha\neq\beta}}^{N} \frac{r_\alpha^4 r_\beta^2}{\left(d_{\alpha\beta}^2 - r_\beta^2\right)^2} \quad , \tag{A.10}$$

where $d_{\alpha\beta}$ represents the distance between the centers of precipitate α and β with the radius r_α and r_β, respectively, and

$$\int_{A_\beta} \left[\left(x-x_\alpha\right)^2 + \left(y-y_\alpha\right)^2\right]^{-2} dxdy = \frac{r_\beta^2}{\left(d_{\alpha\beta}^2 - r_\beta^2\right)^2} \quad , \tag{A.11}$$

has been used, where $\left(x_\alpha, y_\alpha\right)$ represents the position of the center of the precipitate α. Finally, we note that for $\nu_{\text{p}} = \nu_{\text{m}} = \nu$, (A.9) and (A.10) reduce to the expressions (6.3)-(6.6) for two precipitates.

References

Ahniyaz, A., Sakamoto, Y., and Bergstrom, L., (2007) Magnetic Field-Induced Assembly of Oriented Superlattices from Maghemite Nanocubes. *PNAS*, **104**(45), 17570-17574

Alber, I., Bassani, J., Khantha, M. and et. al., (1992) Grain Boundaries as Heterogeneous Systems: Atomic and Continuum Elastic Properties. *Philosophical Transactions of the Royal Society of London A,* **339**, 555-586.

Alber, I., Bassani, J., Vitek, V. and et. al., (1996) Elastic Interfacial Waves in Discrete and Continuous Media. *Physical Review B,* **53**, 8398-8410.

Ardell, A and Nicholson, R (1966) On the Modulated Structure of Aged Ni-Al Alloys. *Acta Metallurgica*, **14** 1295-1306

Budiansky, B. (1965) On Elastic Moduli of some Heterogeneous Materials. *Journal of Mechanics and Physics of Solids*, **13,** 223-227.

Cahn, J., and Hilliard, E., (1958) Free Energy of a Nonuniform System. I. Interfacial Free Energy. *Journal of Chemical Physics*, **28** 258-267.

Chen, L., (2002) Phase-Field Models for Microstructure Evolution. *Annual Review of Materials Research* **32** 113-140.

Doi, M., (1996) Elasticity effects on the microstructure of alloys containing coherent precipitates. *Progress in Material Science*, **40** 79-180

Eggleston, J., McFadden, B., and Voorhees, W., (2001) A Phase-Field Model for Highly Anisotropic Interfacial Energy. *Physica D*, **150**(1) 91-103.

Elder R., Grant M, and Provatas N, et al., (2001) Sharp Interface Limits of Phase-Field Models. *Physical Review* E, **64** 0216

Eshelby, J., (1957) The Determination of The Elastic Field of an Ellipsoidal Inclusion, and Related Problems. *Proceedings of the Royal Society of London series* **241**(1226) 376-396

Eshelby, J., (1961) Elastic Inclusions and Inhomogeneities. *Progress in Solid Mechanics* vol.**2** 89-140

Eshelby, J., (1966) On the Elastic Interaction between Inclusions *Acta Metallurgica*, vol. **14**

1306-1309

Fried, E., and Gurtin, M., Dynamic solid-solid Transitions with Phase Characterized by an Order Parameter. *Physica D* **72** 287-308

Fired, E., and Gurtin, M., Coherent solid-state phase transitions with atomic diffusion: a thermomechanical treatment. *Journal of Statistical Physic*, **95** 1361-1425

Ginzburg, L., and Landau, D., (1950) On the Theory of Superconductivity, *Zhurnal Eksperimental 'Noii Teoreticheskoi Fiziki*, **20**(1) 1064-1082.

Guggenheim, A., (1952) Mixtures: The theory of the equilibrium properties of some simple classes of mixtures, solutions and alloys. *The Clarendon Press*, 270.

Gururajan, M., and Abinadanan, T., (2007) Phase Field Study of Precipitate Rafting under a Uniaxial Stress, *Acta Materialia*, **55**. 5015-5026

Hashin, Z., and Shtrikman, S., (1963) A Variational Approach to the Theory of the Elastic Behaviour of Multiphase Materials, *Journal of the Mechanics and Physics of Solids*, **11**. 127-140.

Hu, S and Chen, L., (2001) A Phase_Field Model for Evolving Microstructures with Strong Elastic Inhomogeneity, *Acta Materials*, **49** 1879-1890

Hung, C., Marshall, F., and Kim, D, (1999) Strain Directed Assembly of Nanoparticle Arrays within a Semiconductor, *Journal of Nanoparticle Research*, **1**. 329-347.

Johnson, W., (1984) On the Elastic Stabilization of Precipitates against Coarsening Under Applied Load, *Acta Metallurgica*, **32**(3) 465-475

Johnson, W., and Wise, M., (2002) Phase Decomposition of a Binary Thin Film on a Patterned Substrate, *Applied Physical Letters*, **81**(5) 919-921

Kawasaki, K., and Enomoto, Y., (1988) Statistical Theory of Ostwald Ripening with Elastic Field Interaction, *Physica A* **150** 463-298

Krill, E.,III, and Chen, L., (2002) Computer Simulation of 3-D Grain Growth using a Phase-Field Model, *Acta Materialia*, **50**(1) 3057-3073.

Larche, F., and Cahn, J., (1982) The Effect of Self-Stress on Diffusion in Solids, *Acta Metallurgica* **30** 1835-1845

Leo, P., Lowengrub, J., and Jou, H., (1998) A Diffuse Interface Model For Microstructural Evolution in Elastically Stressed Solids, *Acta Materialia* **46**(6) 2113-2130

Li, D., and Chen, L., (1998) Computer Simulation of Stress-Oriented Nucleation and Growth of θ' precipitates in Al-Cu Alloys, *Acta Materialia* **46**(8) 2573-2585.

Mori, T., and Tanaka, K., (1973) Average Stress in Matrix and Average Elastic Energy of Materials with Misfitting Inclusions, *Acta Metallurgica*, **21**. 571-574.

Mullins, W., (1957) Theory of Thermal Grooving, *Journal of Applied Physics*, **28**. 333-339.

Mura T., (1982) Micromechanics of defects in solids, *Martinus Nijhoff Publishers*, page 84 and 156.

Patolsky, F., Weizmann, Y. and Lioubashevski, O., (2002) Au-Nanoparticle Nanowires Based on DNA and Polylysine Templates. *Angewandte Chemie - International Edition*, **41**(1). 2323-2327.

Paul, B., (1960) Prediction of Elastic Constants of Multiphase Materials. *Metallurgical Society of American Institute of Mining, Metallurgical and Petroleum Engineers -- Transactions*, **218**. 36-41.

Plass, R., and Kellogg, L., (2000) Surface Morphology Changes during Pb Deposition on Cu(100): Evidence for Surface Alloyed Cu(100)-c(2×2)Pb. *Surface Science*, **470**(1) . 106-120.

Pohl, K., Bartelt, C. and de la Figuera, J., (1999) Identifying the Forces Responsible for Self-Organization of Nanostructures at Crystal Surfaces. *Nature*, **397**(671) 238-241.

Suo, Z., and Lu, W., (2000) Composition Modulation and Nanophase Separation in a Binary Epilayer. *Journal of the Mechanics and Physics of Solids*, **48**. 211-232.

Thornton, K., Agren, J., and Voorhees, W., (2003) Modeling the Evolution of Phase Boundaries in Solids at the Meso- and Nano-Scales. *Acta Materialia*, **51**(1) 5675-5710.

Vaithyanathan, V., and Chen, Q., (2002) Coarsening of Ordered Intermetallic Precipitates with Coherency Stress. *Acta Materialia*, **50**(1). 4061-4073.

Van Der Vorst, A., (1992) Bi-CGSTAB: A Fast and Smoothly Converging Variant of Bi-CG for the Solution of Nonsymmetric Linear Systems. *SIAM Journal on Scientific and Statistical Computing*, **13**. 631-644.

Velev, D., Prevo, G., and Bhatt, H., (2003) On-Chip Manipulation of Free Droplets. *Nature*, **426** (696) 515-516.

Wen ,H., Wang, B., Simmons, J.P., (2006) A Phase-Field Model for Heat Treatment Applications

in Ni-Based Alloys *Acta Materialia* **54** 2087-2099

Wheeler, A., Boettinger, W and McFadden, G., (1992) Phase-Field Model for Isothermal Phase Transitions in Binary Alloys *Physical Review A* **45**(10) 7424-7439

Willis, R., (1977) Bounds and Self-Consistent Estimates for the overall Properties of Anisotropic Composites *Journal of the Mechanics and Physics of Solids*, **25**. 185-202.

Wise, S., Kim, J., and Johnson, W., (2005) Surface-Directed Spinodal Decomposition in a Stressed, Two-Dimensional, Thin Film. *Thin Solid Films*, **473**, 151-163

Wu, Y., Cui, Y., and Huynh, L., (2004) Controlled Growth and Structures of Molecular-Scale Silicon Nanowires. *Nano Letters*, **4**. 433-436.

Zhu, J., Chen, L., and Shen, J., (2001) Morphological Evolution during Phase Seperation and Coarsening with Strong Inhomogeneous Elasticity, *Modeling Simulation Material Science Engineering* **9** 499-511

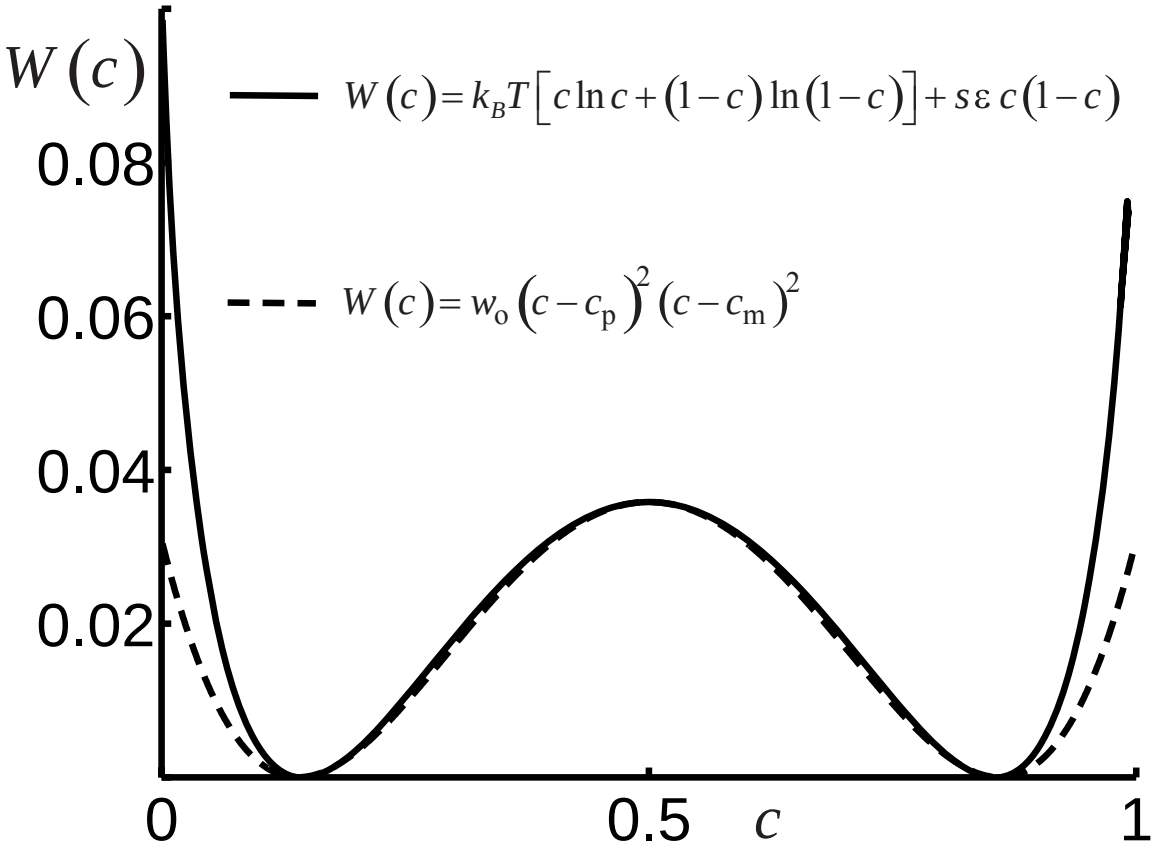

Figure 1. Two representations of the chemical energy.

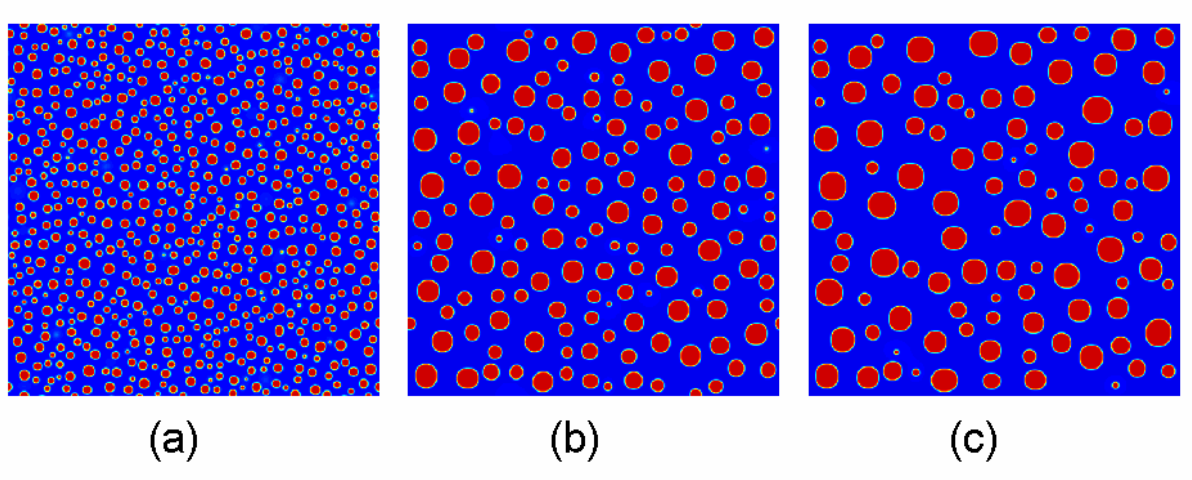

Figure 2. Bulk aggregation: (a) short-time, (b) intermediate-time, and (c) long-time concentration fields for $\varepsilon^{\mathrm{T}} = 0.5\%$ and $\kappa = 1$. The deepest blue represents regions that are depleted of solute and red denotes the precipitate phase.

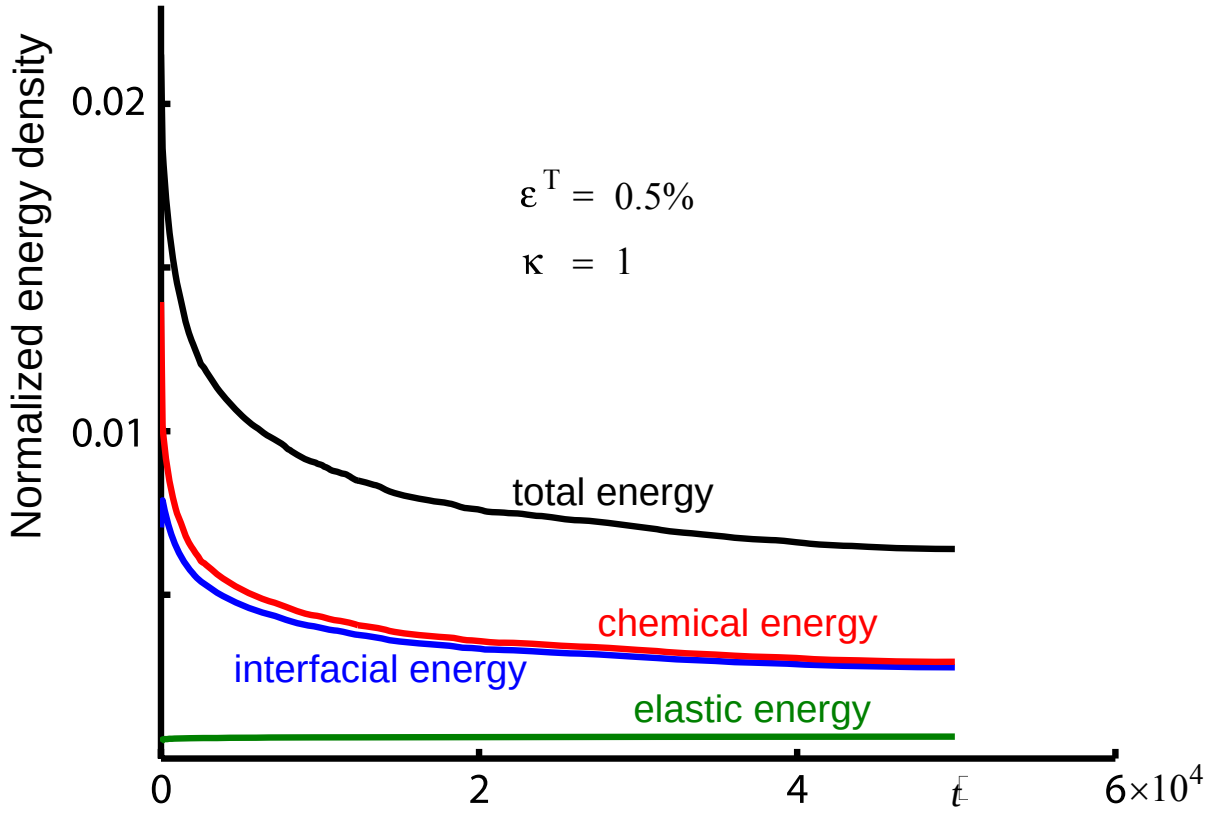

Figure 3. Average energy densities normalized by $2w_o\left(c_p - c_m\right)^2$ as a function of normalized time given by (4.3) with (4.4).

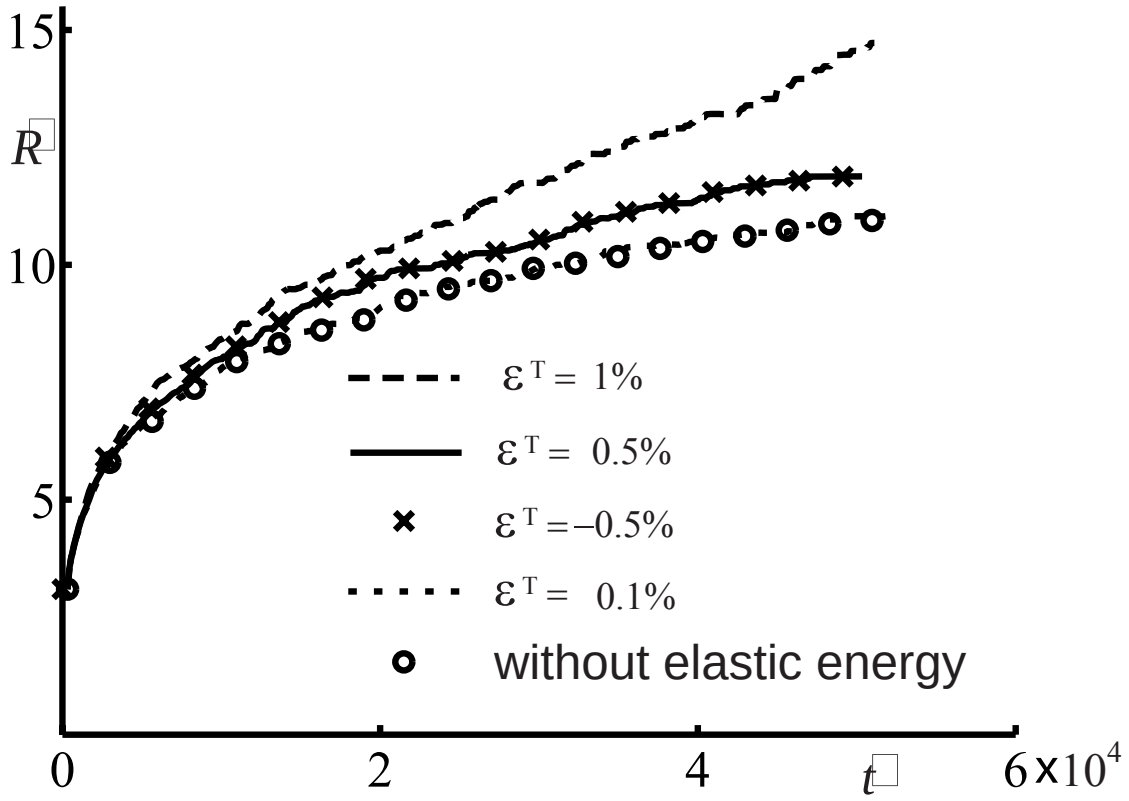

Figure 4. The evolution of the average dimensionless radius as a function of normalized time ($\kappa = 1$). Note: the results for $\varepsilon^{T} = -0.5\%$ and 0.5% are nearly indistinguishable.

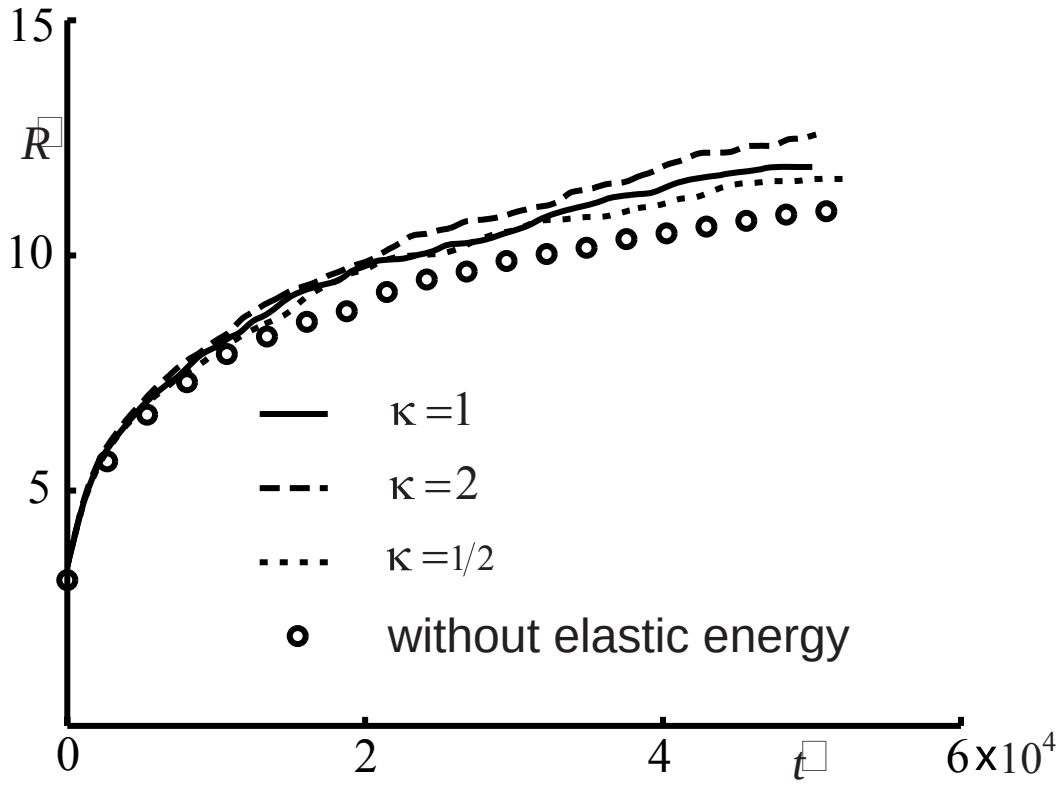

Figure 5. The evolution of average dimensionless radius as a function of normalized time ($\varepsilon^{T} = 0.5\%$).

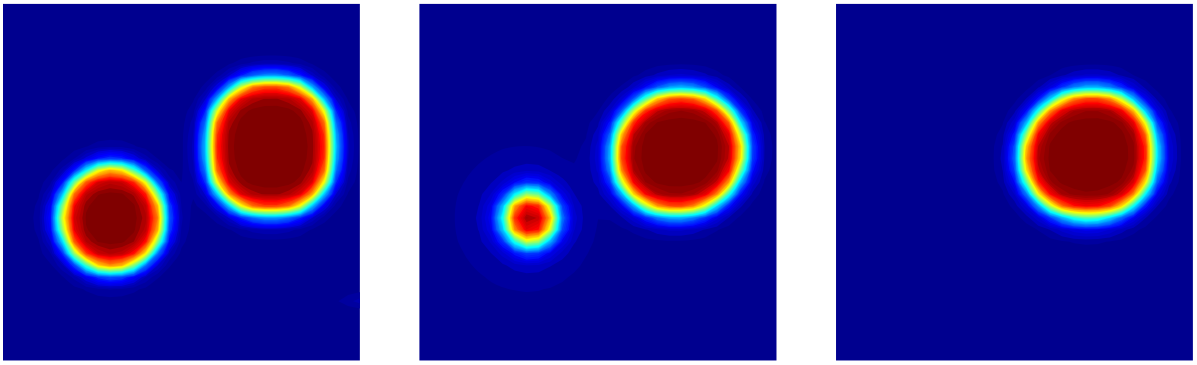

Figure 6. Two-particle system: (a) initial, (b) intermediate, and (c) equilibrium concentration fields.

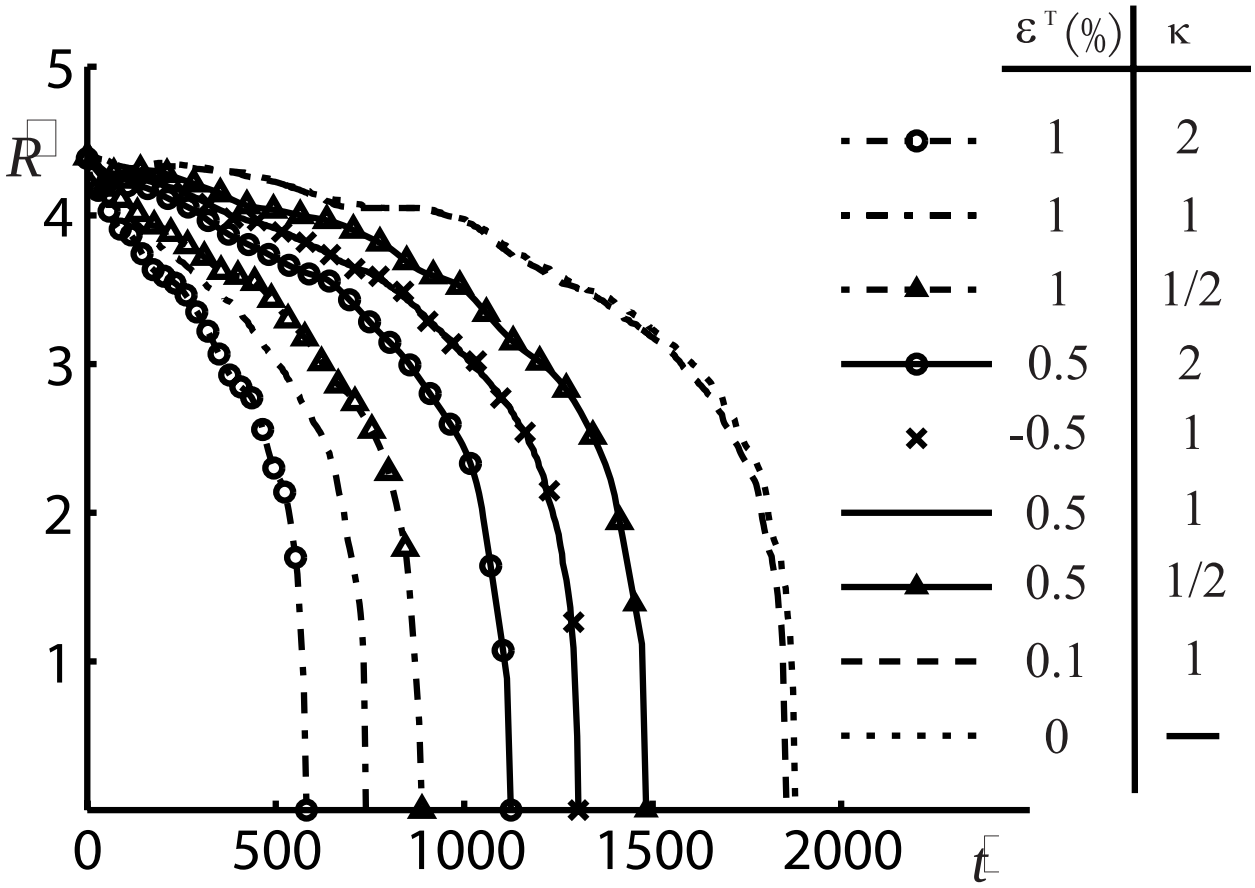

Figure 7. Dimensionless radius of the smaller particle as a function of normalized time. Note: the results for $\varepsilon^{T} = -0.5\%$ and 0.5% with $\kappa = 1$ are nearly indistinguishable.

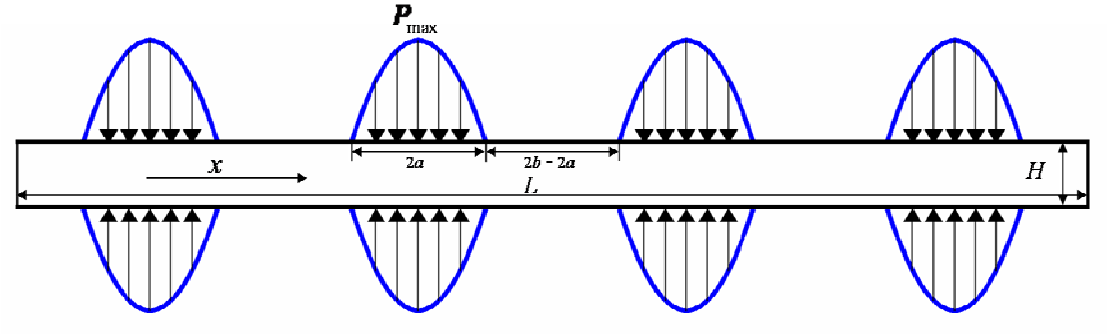

Figure 8. Periodic indentation.

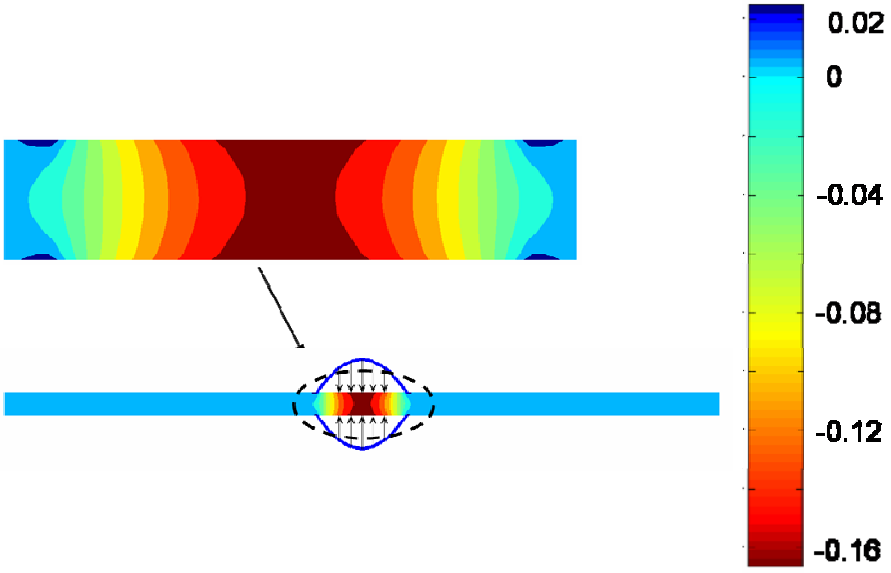

Figure 9. The mean stress, $\sigma_{kk}/3$, normalized by $2w_{\mathrm{o}}\left(c_{\mathrm{p}}-c_{\mathrm{m}}\right)^{2}$, for a homogeneous film with $\varepsilon^{\mathrm{T}}=0$ and $\kappa=1$ and a normalized $\hat{P}_{\max}=-0.5$. The deepest red regions are under highest compression and blue regions are slightly tensile.

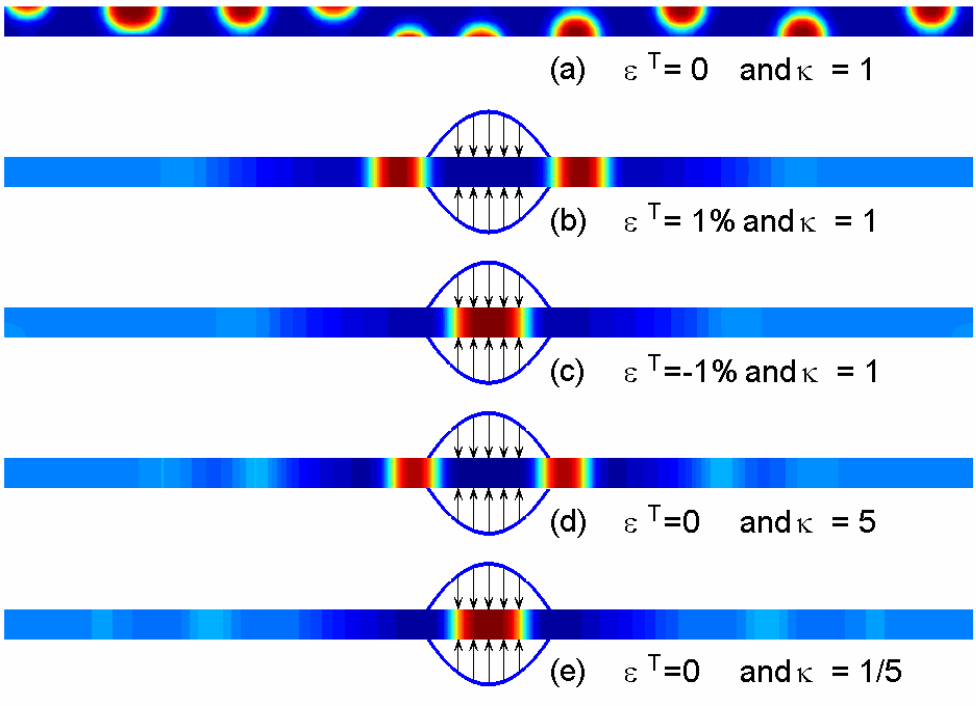

Figure 10. Concentration fields ($\hat{t} \approx 500$) for a thin film under a quadratically-varying traction.

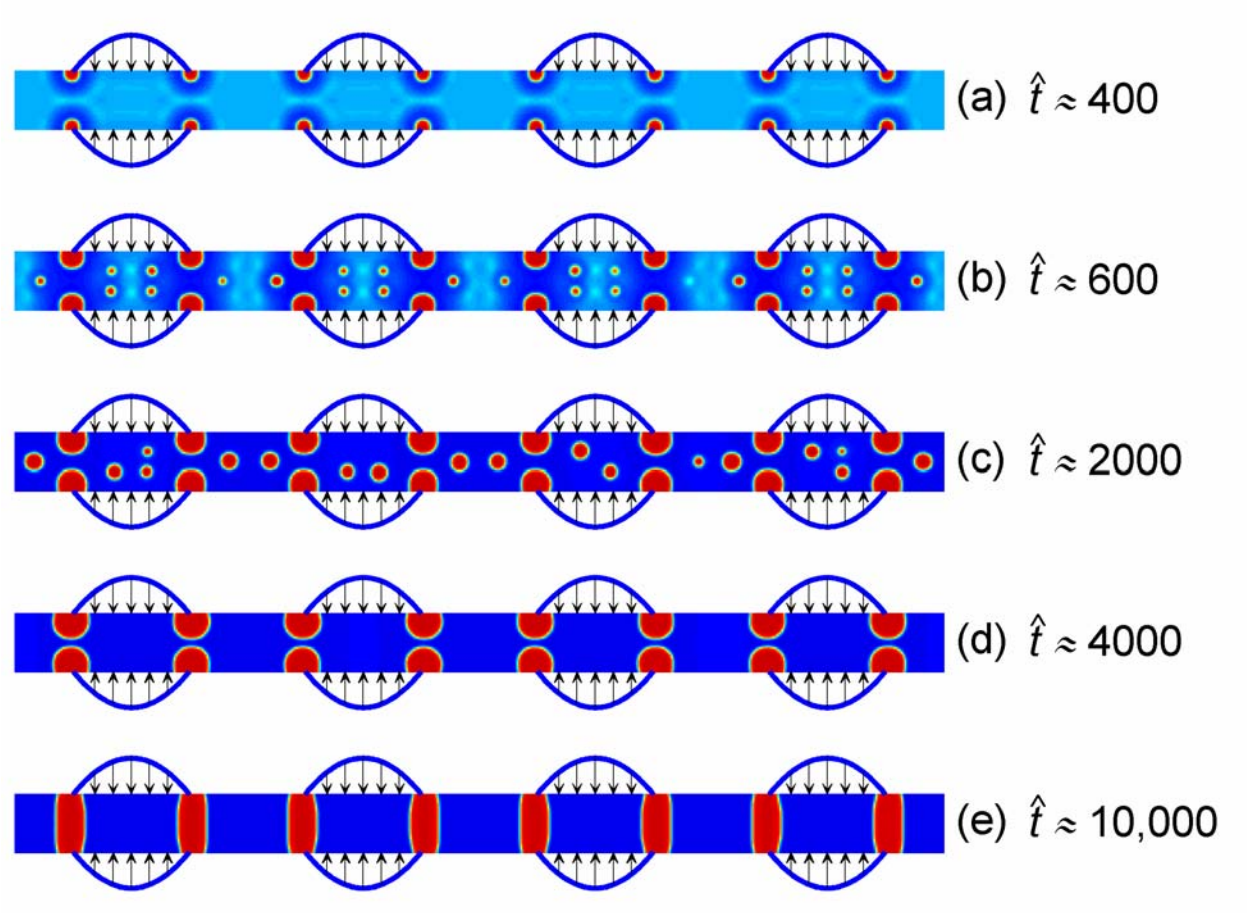

Figure 11. Thin film under periodically-patterned external load with $\varepsilon^{\mathrm{T}} = 1\%$ and $\kappa = 1$: (a) and (b) short-time, (c) and (d) intermediate-times, and (e) long-time concentration fields. There is no observable change from (e) up to $\hat{t} \approx 40,000$.

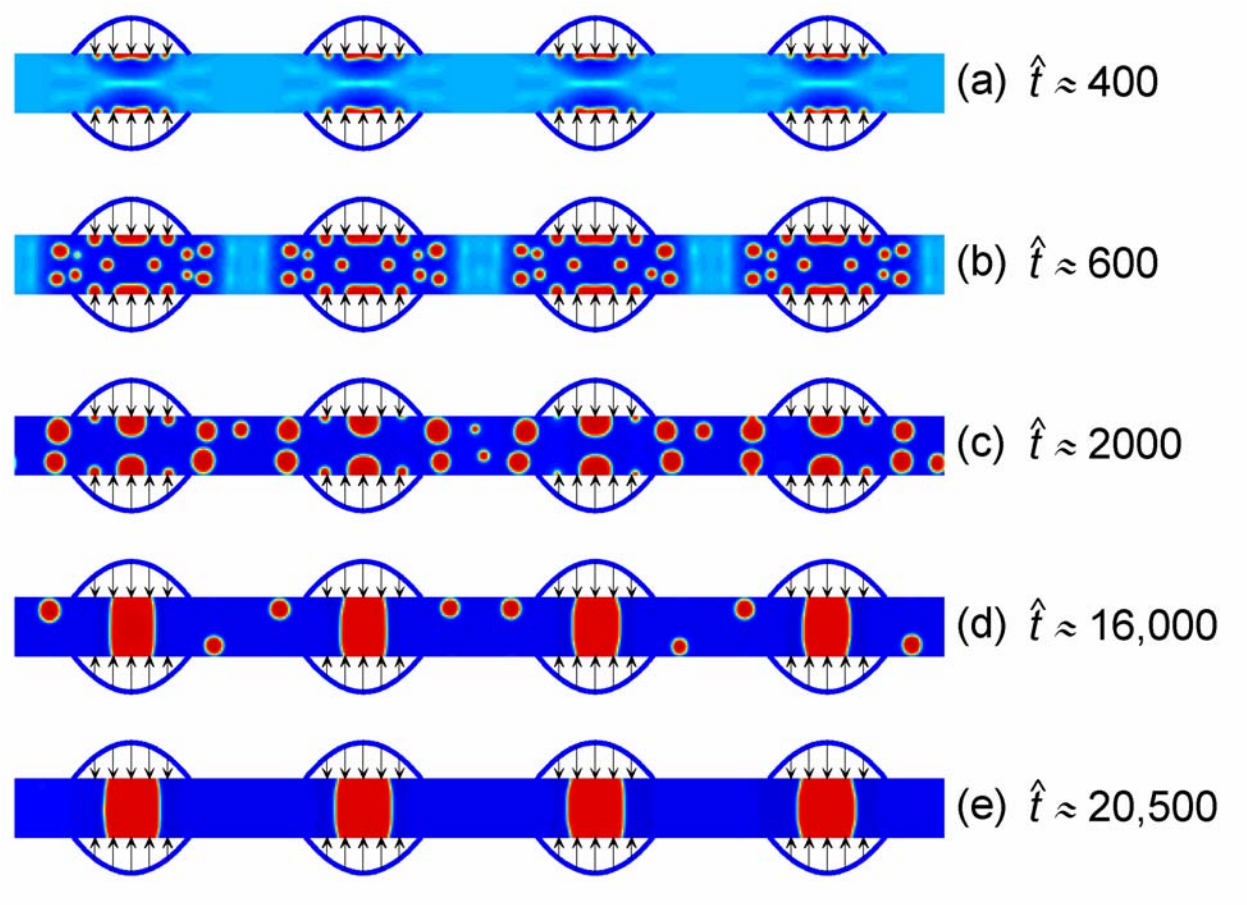

Figure 12. Thin film under periodically-patterned external load with $\varepsilon^{\mathrm{T}} = -1\%$ and $\kappa = 1$: (a) and (b) short-time, (c) and (d) intermediate-times, and (e) long-time concentration fields. There is no observable change from (e) up to $\hat{t} \approx 40,000$

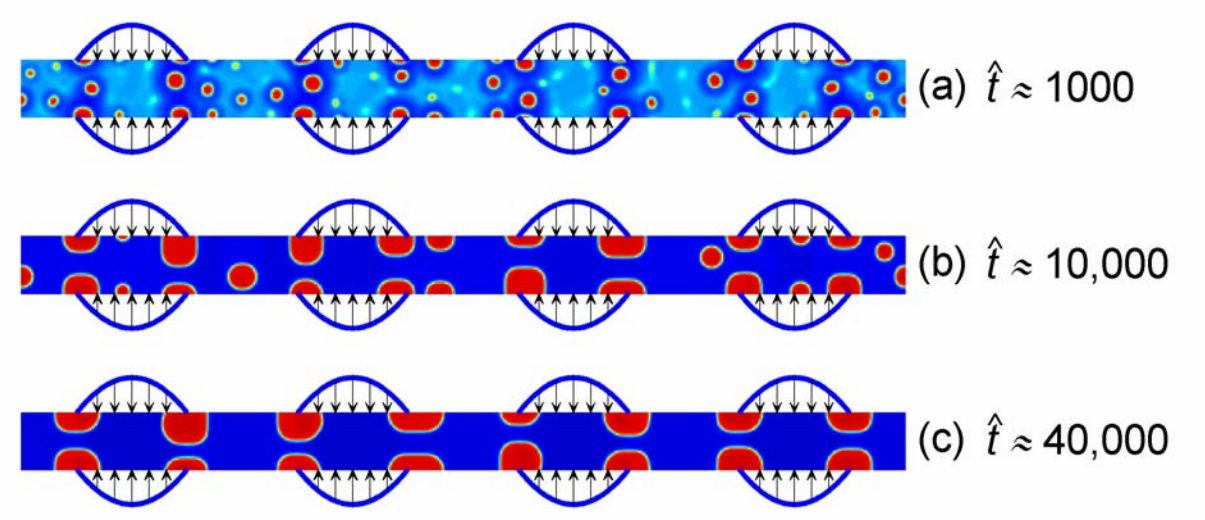

Figure 13. Thin film under periodically-patterned external load with $\varepsilon^{\mathrm{T}} = 0$ and $\kappa = 5$: (a) short-time, (b) intermediate-times, and (c) long-time concentration fields. There is no observable change from (c) up to $\hat{t} \approx 10^6$.

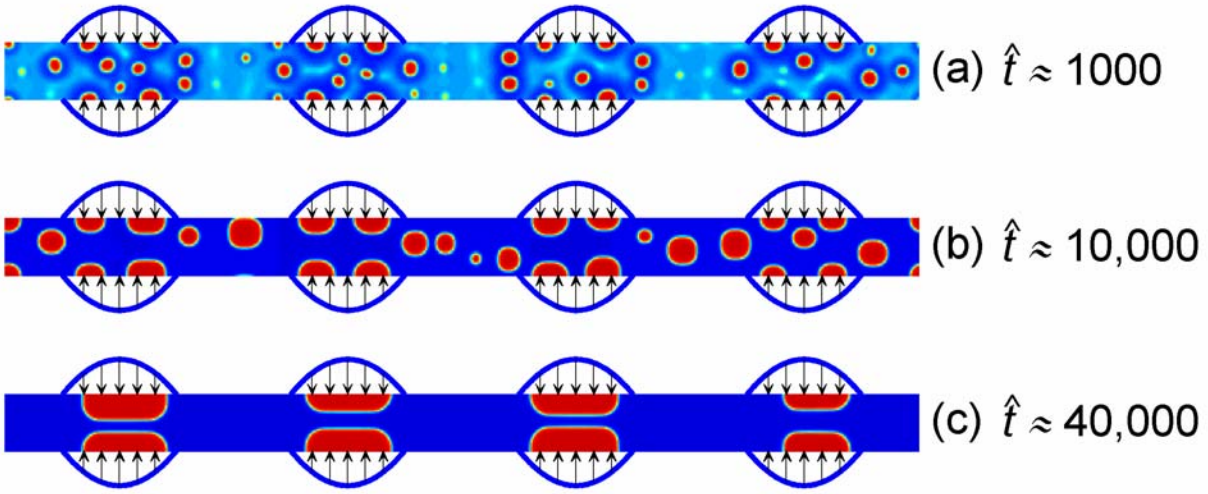

Figure 14. Thin film under periodically-patterned external load with $\varepsilon^{\mathrm{T}} = 0$ and $\kappa = 1/5$: (a) short-time, (b) intermediate-times, and (c) long-time concentration fields. There is no observable change from (c) up to $\hat{t} \approx 10^6$.